Driving axon regeneration by orchestrating neuronal and non-neuronal innate immune responses via the IFNγ-cGAS-STING axis

Xu Wang[1,2,3,4,5,6,11], Chao Yang[1,2,3,4,5,6,11], Xuejie Wang[1,2], Jinmin Miao[7], Weitao Chen[4], Yiren Zhou[1], Ying Xu[1,8], Yongyan An[1], Aifang Cheng[3,9], Wenkang Ye[3,9], Mengxian Chen[1], Dong Song[1,8], Xue Yuan[2], Jiguang Wang[1,8], Peiyuan Qian[3,9], Angela Ruohao Wu[1,3,8,10], Zhong-Yin Zhang[7], Kai Liu[1,2,3,4,5,6,12,*]

[1]Division of Life Science, State Key Laboratory of Molecular Neuroscience, The Hong Kong University of Science and Technology, Hong Kong, China

[2]Hong Kong Center for Neurodegenerative Diseases, Hong Kong, China

[3]Southern Marine Science and Engineering Guangdong Laboratory (Guangzhou), Guangzhou, China

[4]Biomedical Research Institute, Shenzhen Peking University–The Hong Kong University of Science and Technology Medical Center, Shenzhen 518036, China

[5]Guangdong Provincial Key Laboratory of Brain Science, Disease and Drug Development, HKUST Shenzhen Research Institute, Shenzhen-Hong Kong Institute of Brain Science, Shenzhen, Guangdong 518057, China

[6]Guangdong-Hong Kong-Macao Greater Bay Area Center for Brain Science and Brain-Inspired Intelligence, Guangzhou 510515, China

[7]Department of Medicinal Chemistry and Molecular Pharmacology, Department of Chemistry, Center for Cancer Research and Institute for Drug Discovery, Purdue University, West Lafayette, IN, USA

[8]Department of Chemical and Biological Engineering, The Hong Kong University of Science and Technology, Hong Kong, China

[9]Department of Ocean Science, The Hong Kong University of Science and Technology, Hong Kong, China

*Correspondence: kailiu@ust.hk.

DECLARATION OF INTERESTS

The authors declare no competing interests.

[10]Center for Aging Science, The Hong Kong University of Science and Technology, Hong Kong, China

[11]These authors contributed equally

[12]Lead contact

SUMMARY

The coordination mechanism of neural innate immune responses for axon regeneration is not well understood. Here, we showed that neuronal deletion of protein tyrosine phosphatase non-receptor type 2 sustains the IFNγ-STAT1 activity in retinal ganglion cells (RGCs) to promote axon regeneration after injury, independent of mTOR or STAT3. DNA-damage-induced cGAMP synthase (cGAS)-stimulator of interferon genes (STINGs) activation is the functional downstream signaling. Directly activating neuronal STING by cGAMP promotes axon regeneration. In contrast to the central axons, IFNγ is locally translated in the injured peripheral axons and upregulates cGAS expression in Schwann cells and infiltrating blood cells to produce cGAMP, which promotes spontaneous axon regeneration as an immunotransmitter. Our study demonstrates that injured peripheral nervous system (PNS) axons can direct the environmental innate immune response for self-repair and that the neural antiviral mechanism can be harnessed to promote axon regeneration in the central nervous system (CNS).

Graphical abstract
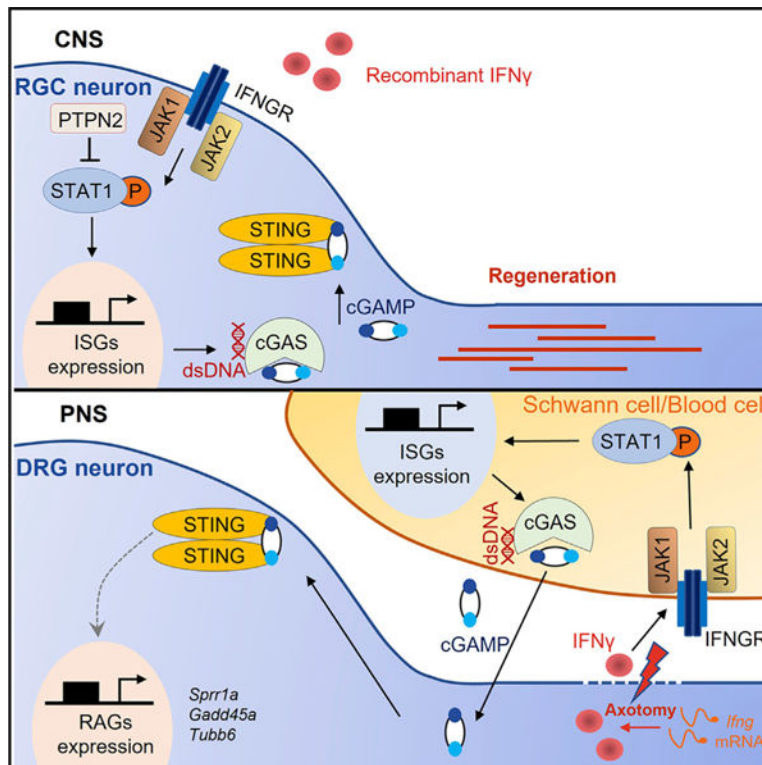
In brief

The neural innate immune responses for axon regeneration is not well understood. Wang and Yang et al. demonstrate that activating the immune signaling IFNγ-cGAS-STING axis promotes axon regeneration in both the PNS and the CNS, uncovering a role for the antiviral machinery in neural repair.

INTRODUCTION

Neurotrauma in the adult mammalian central nervous system (CNS), such as spinal cord injury, leads to devastating and persistent neurological deficits. When axonal damage occurs without efficient axon regeneration, despite many neurons surviving the damage, neural networks become disconnected and paralysis results. In contrast, in the peripheral nervous system (PNS), the dorsal root ganglion (DRG) neurons can spontaneously regenerate their peripheral axons after nerve injury. Comparing the regeneration processes between the CNS and PNS has helped us understand why CNS axons fail to regenerate.[1–7] In addition to the intrinsic growth capability of the CNS neurons and the extrinsic environment,[8–12] the innate immune response is also critical for axon regeneration.[13] Studies in the PNS support the notion that distant nerve injuries elicit inflammatory responses not only in the local environment but also in remote neurons, even before immune cells infiltrate into the lesion site.[14] Peripheral axotomy enhances neuronal SARM1,[15] axonal STAT3,[16] and neuronal STAT3[17] in DRG neurons, which is indicative of an intrinsic immune reaction in neurons after injury. Contrastingly in the CNS, optic nerve injuries increase ciliary neurotrophic factor (*Cntf*) gene expression only transiently in retinal ganglion cells (RGCs),[18] which is not sufficient for axon regeneration. Another study found that inducing inflammation within the retina by directly injecting zymosan, a fungal cell wall extract, can induce infiltration and activation of macrophages and neutrophils in the eye. The increased cytokines and growth factors produced by immune cells were found to promote axon regeneration.[19–21] Understanding the different regulatory mechanisms of the neuronal and non-neuronal innate immune responses between CNS and PNS will help development of strategies to facilitate neural repair.

As a critical cytokine regulating innate immunity against viruses and bacteria, interferon-gamma (IFNγ) is predominantly produced by lymphocytes.[22] However, the function of IFNγ during neurotrauma and regeneration is still under debate,[23] largely because most studies have used approaches such as germline knockout (KO) or systemic ligand administration that cannot separate IFNγ signaling in neurons from non-neuronal cells. Recently, accumulating evidence has shown that IFNγ directly participates in neuronal development. Transient IFNγ treatment of human iPSC-derived neural progenitors increased neurite length.[24] Janus kinases 2-signal transducer and activator of transcription proteins 1(JAK2-STAT1) signaling drives the elimination of inactive synaptic connections in the brain.[25] Moreover, *Ifng*- or *Stat1*-KO mice exhibit social deficits and abnormal neuronal connectivity.[26] However, how neuronal IFNγ signaling and its downstream contribute to the axon elongation and regeneration remains poorly understood.

IFNγ binds with the interferon gamma receptor (IFNGR) complex and upregulates the downstream interferon-stimulated genes (ISGs) by the JAK-STAT signaling pathway. The

cyclic guanosine monophosphate-adenosine monophosphate (cGAMP) synthase (cGAS), one of the intracellular pattern recognition receptors (PRRs), and stimulator of interferon genes (STINGs) are also ISGs transcriptionally induced by interferon-STAT1 activation through a positive feedback mechanism.[27,28] The cGAS-STING pathway has emerged as a key regulator against pathogens.[29] Once bound to exogenous DNA, the catalytic activity of cGAS leads to the production of $2',3'$-cGAMP, a cyclic dinucleotide as an innate agonist of STING. Then, the STING oligomers recruit tank-binding kinase 1 (TBK1) and interferon regulatory factor 3 (IRF3), leading to the expression of type I interferon (IFN-I). In addition, neurodevelopment also requires activating the cGAS-STING pathways. STING deletion was found to reduce neuronal differentiation and leads to autistic-like behaviors in mice.[30] Recently, it has been reported that STING functions as a critical regulator of nociception in DRG,[31] indicating its additional role beyond immune regulation. However, the role of the cGAS-STING pathway in axon regeneration remains unclear.

Here, we found that protein tyrosine phosphatase non-receptor type 2 (*Ptpn2*) inhibition combined with low-dose IFNγ enhances CNS axon regeneration by amplifying IFNγ-STAT1 signaling, with the cGAS-STING pathway as the functional downstream signaling. In the PNS, the IFNγ-cGAS-STING axis is coordinated by both neuronal and non-neuronal cells to support spontaneous axon regeneration.

RESULT

PTPN2 inhibits axon regeneration

We used the DRG replating assay as a screening system to search for intrinsic suppressors of axon growth.[32,33] Several phosphatases have been identified as suppressors of axon regeneration,[34–36] and they are also viable targets for therapeutic development.[37] To identify phosphatases that inhibit axon elongation, we collected a list through the Dharmacon mouse short hairpin RNA (shRNA) library targeting phosphatases and arrived at ~84 genes that were confirmed to be expressed in the brain by the *in situ* Allen brain atlas. We knocked down individual genes using shRNA in isolated adult DRG neurons by electroporation, cultured them for 3 days and did replating to evaluate the axon elongation in 24 h. We found that five phosphatase genes inhibited axon growth, including previously identified *Pten* and *Ptprf* (Figures 1A and 1B), with verified knockdown efficacy (Table S1). In parallel, we also conducted screening using a panel of specific protein tyrosine phosphatase inhibitors (Tables S2 and S3) with defined selectivity and efficacy.[37–44] Interestingly, PTPN2 was also identified (Figures 1C and 1D). We subsequently used the optic nerve injury model to assess the effect of PTPN2 inhibition *in vivo*. Directly injecting the PTPN2 inhibitor[43] into the vitreous humor of adult wild-type (WT) mice elicited modest axon regeneration at 2 weeks after optic nerve crush in a dose-dependent manner (Figures 1E and 1F), with RGC survival not affected (Figure S1A). To confirm, we generated *Ptpn2* floxed mice (Figure S1B). The KO efficacy was verified by injecting adeno-associated virus carrying Cre recombinase (AAV-Cre) into the neonatal mouse cortex and performing western blotting of the cortical tissue (Figures S1C and S1D). Consistent with the shRNA transfection result, the deletion of *Ptpn2* in cultured DRG neurons by AAV-Cre increased the axon elongation (Figures S1E and S1F). Next, we injected AAV-hSyn-Cre into the eyes of adult *Ptpn2* floxed

mice to induce conditional KO (cKO) in RGCs. Then, we performed optic nerve crush and assessed axon regeneration. We found RGC survival rates to be comparable between the control and KO groups (Figures S1G and S1H). Cholera toxin b subunit (CTB) labeling of the optic nerves showed modestly more regenerating axons in mice injected with AAV-Cre than in the control mice (Figures 1G and 1H). The results from the PTPN2 inhibitor and KO experiments indicated that PTPN2 plays an inhibitory role in axon regeneration *in vivo*.

IFNγ boosts *Ptpn2* cKO-induced axon regeneration and synergizes with *Pten/Socs3* codeletion

We sought to explore the transcriptional effect of *Ptpn2* deletion in injured neurons and generated tamoxifen-inducible conditional KO of *Ptpn2* in DRG neurons by crossing Advillin-CreERT2 with *Ptpn2* floxed mice (*Ptpn2* cKO). We designed an RNA sequencing (RNA-seq) experiment comparing the transcriptomes in DRGs either intact or at 3 days post crush (dpc) (WT intact, WT 3 dpc, *Ptpn2* cKO intact and *Ptpn2* cKO 3 dpc). To elucidate which signaling pathway was activated in *Ptpn2* cKO DRGs after injury, we first identified the differentially expressed genes (DEGs, fold change > 2, p adjust < 0.1) in cKO 3 dpc group by comparing with the WT 3 dpc group. Gene Ontology analysis showed that the upregulated genes were significantly enriched in the categories related to host defense responses and interferon-related signaling (Figure S1I). We found that 39 of 78 ISGs[45–47] expressed in DRGs were upregulated in cKO injury compared with WT injury. However, only 6 of 78 ISGs were upregulated in cKO intact compared with WT intact (Figure S1J). This result suggested that *Ptpn2* deletion interacted with injury signals to enhance ISG signaling in DRG neurons.

To assess whether exogenous ligands can further enhance the axon regeneration induced by *Ptpn2* deletion, we injected individual candidate recombinant proteins or peptides into the eyes of *Ptpn2* KO mice at the time of optic nerve crush. In 2 weeks, low-dose IFNγ, but not leptin, insulin, epidermal growth factor (EGF), or nerve growth factor (NGF), significantly boosted axon regeneration (Figure S2A). We repeated the experiment and found that while IFNγ alone induced modest regrowth, IFNγ plus *Ptpn2* KO elicited robust regeneration (Figures 1A and 1B). The RGC survival rates were comparable among the four groups (Figure S2B). Next, we hypothesized that axon regeneration induced by *Ptpn2* cKO without exogenous IFNγ requires endogenous IFNγ. We first performed western blotting to examine the expression level of endogenous IFNγ in the mouse eye. Interestingly, IFNγ was detected in the vitreous humor, but not in the retina or the optic nerve (Figure S2C). Then we investigated whether endogenous IFNγ contributes to axon regeneration. It is known that the type II interferon IFNγ activates cellular responses through its interactions with a heterodimeric receptor consisting of IFNGR1and IFNGR2; both receptors are required to elicit the full function of IFNγ signaling. We generated AAVs expressing either *Ifngr1* shRNA (sh-*Ifngr1*) or *Ifngr2* shRNA (sh-*Ifngr2*) and injected them into mouse eyes to decrease the level of the IFNGR complex in RGCs. We found that knocking down either receptor by AAV-*Ifngr1* or *Ifngr2* shRNA almost completely suppressed *Ptpn2* cKO-induced axon regeneration (Figures 2C and 1D). Our data demonstrated that endogenous IFNγ is essential for axon regeneration induced by *Ptpn2* KO neurons. In addition, we found that exogenous IFNb, one of the IFN-I, enhanced *Ptpn2* cKO-induced axon regeneration (Figures

S2D and S2E), with weaker effect than IFNγ. The results indicated that both type I and type II interferons stimulate regeneration induced by *Ptpn2* cKO. We focused on IFNγ for further studies.

One of the major challenges in the field is to elicit rapid and long-distance axon regeneration, which is very difficult to achieve by single gene manipulation. *Pten*/*Socs3* codeletion in RGC promotes robust axon regeneration and synaptic reconnection after optic nerve or optic tract lesions.[48–50] To further enhance the regrowth induced by *Pten*/*Socs3* codeletion, we generated *Pten*/*Socs3*/*Ptpn2* triple-floxed mice. We injected AAV-Cre into the vitreous body of *Pten*/*Socs3* double-floxed or *Pten*/*Socs3*/*Ptpn2* triple-floxed mice to achieve double or triple KO of the floxed genes in RGCs, with or without AAV-CNTF. At the time of injury, we injected vehicle or IFNγ into the *Pten*/*Socs3* mutant and the *Pten*/*Socs3*/*Ptpn2* mutant. At 2 weeks after injury, CTB labeling showed a very significant increase in axon regeneration in the triple KO groups injected with AAV-CNTF and IFNγ (Figure 2E). A synergistic effect was observed at 1 mm or longer distal to the lesion site (Figure 2F). The enhanced growth continued at 4 weeks, and about 3-fold more axons could be found at the optic chiasm (Figures S2F and S2G). Thus, IFNγ boosted the *Ptpn2* cKO effect and synergized with *Pten*/*Socs3* codeletion.

Neuronal *Ptpn2* deletion amplifies IFNγ response and sustains STAT1 activation to promote axon regeneration

To investigate the mechanism by which IFNγ stimulated axonal regeneration of RGCs upon *Ptpn2* deletion, we performed retrograde labeling of RGCs, isolated RGCs by cell sorting, and conducted RNA-seq (Figure S3A) at 3 dpc. Analysis showed that ISGs were among the most prominently affected (Figure S3B). ISGs are commonly expressed in the immune cells in response to viral infection, and our data showed that ISGs could also be induced in RGCs (Figure S3C). Consistent with low level of endogenous IFNγ stimulation, heatmap showed that most of ISGs were induced by cKO+ exogenous IFNγ but not cKO only (Figure S3D). Then, we evaluated whether the growth effect induced by *Ptpn2* KO plus IFNγ was IFNGR dependent. In mice with *Ptpn2* KO plus IFNγ, *Ifngr1*, or *Ifngr2* KD evidently suppressed the enhanced axon regeneration of the injured optic nerve (Figure 2A). Since interferon-a/b receptor subunit 1 (IFNAR1) and interferon-a/b receptor subunit 2 (IFNAR2) form the IFNAR complex that is activated by IFN-I, but not by IFNγ, we included AAVs carrying sh-*Ifnar1* or sh-*Ifnar2* as controls. As expected, *Ifnar1* and *Ifnar2* KD did not affect the regrowth (Figure 2A). These data suggest that IFNγ stimulates axon regeneration specifically through its ligand-receptor interaction. Thus, neuronal *Ptpn2* deletion amplifies the IFNγ response in RGCs to promote axon regeneration.

We next examined how the downstream signaling is amplified and contributes to the axon regeneration induced by *Ptpn2* KO plus IFNγ. Canonically, IFNGR engaged by IFNγ leads to the activation of JAK1 and JAK2 and the subsequent phosphorylation of STAT1 and STAT3. Phosphorylated STAT1 (p-STAT1) and STAT3 translocate to the nucleus and stimulate the transcription of target genes. By performing immunostaining, we found that p-STAT1 was barely detectable in WT RGCs. IFNγ administration induced p-STAT1 accumulation in the nuclei of WT RGCs at 1 dpc but not at 3 dpc (Figure 3B). In contrast,

p-STAT1 was enhanced up to 5 dpc in the *Ptpn2* KO + IFNγ group (Figures 3B and S3E), consistent with previous findings that PTPN2 negatively regulates STAT1 signaling by dephosphorylating STAT1;[51,52] p-STAT3 was also activated (Figure S3F). It has been shown that GP130-STAT3 signaling mediates the regeneration induced by CNTF,[18,50] and the mammalian target of rapamycin (mTOR) signaling is the central mediator of axon regeneration induced by *Pten* deletion.[36] To investigate which STAT(s) may mediate the growth and whether this effect has any crosstalk with mTOR, we carried out loss-of-function experiments using *Ptpn2* shRNA combined with either conditional KO for *Jak1*, *Stat3*, *mTOR*, or shRNA knockdown for *Stat1*. We found that either *Jak1* cKO or *Stat1* KD almost completely blocked the regeneration, but neither *Stat3* cKO nor *mTOR* cKO showed any significant suppression of the regrowth (Figures 3C and 2D). In retinal cells, over 90% Tuj1+ RGCs but not glial cells were infected by AAV2-Ptpn2-shRNA (Figures S3G and S3H), consistent with previous reports.[53] In addition, *Ifngr1* cKO in RGCs suppressed the axon regeneration induced by *Ptpn2* shRNA+ IFNγ (Figure S3I). Our data showed that AAV2-Ptpn2-shRNA largely affected RGCs in the retina and the regeneration induced by *Ptpn2* shRNA+ IFNγ also required neuronal interferon signaling, consistent with the result of *Ptpn2* KO + IFNγ. Then, we evaluated whether neuronal IFNγ signaling is involved in the regeneration induced by AAV-CNTF. Neither *Stat1* KD (Figures 3E and 3F) nor *Ifngr* deletion (Figure S3J) decreased the regeneration induced by AAV-CNTF, which was largely suppressed by *Stat3* cKO (Figures 2E and 2F).

In conclusion, *Ptpn2* KO plus IFNγ promotes axon regeneration mainly through the IFNGR-JAK1-STAT1 signaling axis, distinct from the STAT3 or mTOR pathway. The combination of three independent mechanisms likely contributes to the observed synergy produced by the triple KO of *Pten*, *Socs3*, and *Ptpn2*. A cocktail therapy based on the mTOR, STAT3, and STAT1 combination can be considered in future studies.

The cGAS-STING pathway is essential for the regeneration induced by *Ptpn2* deletion plus IFNγ

Since the critical role of STAT1 activation in the regeneration is consistent with our RNA-seq data on the upregulation of many ISGs, we speculated that ISGs could be functionally linked with the regeneration. In macrophages, PTPN2 negatively regulates the cGAS-STING pathway.[54] cGAS and STING are also ISGs transcriptionally induced by interferon-STAT1 activation through a positive feedback mechanism.[27,28] After sensing cytosolic double-strand DNA, cGAS is activated and catalyzes the production of the second messenger cGAMP, which binds to and activates STING.[29] We examined whether cGAS-STING signaling is involved in the regeneration effect. By performing western blotting, we found that cGAS was detectable only in mouse retinas with *Ptpn2* cKO plus IFNγ at 1 dpc (Figure S4A), when p-STAT1 was most elevated among all groups (Figure S4B). With immunostaining, we also verified that cGAS was upregulated in RGCs at 2 dpc in mice with *Ptpn2* cKO plus IFNγ but not in the PBS, IFNγ-only, or *Ptpn2*-cKO-only group (Figures 4A and 4B). Then we investigated the endogenous source of DNA for cGAS activation in RGCs. DNA damage can generate cytoplasmic DNA to activate cGAS.[55] Phosphohistone H2A.X (pH2A.X), a DNA damage and repair marker, could not be detected in non-injured retina with control or IFNγ injection only, but in a small percentage of

RGCs after nerve injury (Figures S4C and S4D). Surprisingly, *Ptpn2* deletion could induce pH2A.X in 80% of RGCs even without injury. *Ptpn2* KO, IFNγ and nerve injury together did not further increase the percentage of pH2A.X-positive RGCs (Figures S4C and S4D). We also confirmed that DNA damage occurred in injured RGCs and *Ptpn2* cKO RGCs by doing Comet assay on fluorescence-activated cell sorting (FACS)-sorted RGCs, in which a comet tail could be observed around the nucleus by electrophoresis (Figures S4E and S4F). As a positive control, DNA topoisomerase I inhibitor camptothecin (CPT) was used to induce DNA damage in RGCs. Next, we asked whether cytoplasmic double stranded DNA (dsDNA) was increased by DNA damage in RGCs. By immunostaining with specific antibodies recognizing dsDNA and a mitochondria marker, TOMM20, we found that in control WT RGCs dsDNA was mainly restricted in nucleus and mitochondria (Figures 4C and 4D). In *Ptpn2* cKO RGCs, dsDNA staining could be detected in cytoplasm outside the mitochondria (Figures 3C and 3D). As the positive control, CPT treatment increased cytoplasmic dsDNA in RGCs. Furthermore, knocking down *Stat1* significantly decreased cGAS upregulation in injured RGCs induced by *Ptpn2* cKO + IFNγ (Figure S4G). Thus, we provided evidence to support that upregulated cGAS may be activated by DNA-damage-induced cytoplasmic dsDNA in RGCs. Next, we injected AAV-shRNA-*Ptpn2* into *Cgas*, *Sting*, or *Mavs* (mitochondrial antiviral signaling protein) KO mice to knock down *Ptpn2* in RGCs and assessed the optic nerve regeneration by IFNγ stimulation. Distinct from STING, MAVS is an adapter protein that transduces signals from cytosolic RNA sensors. At 2 weeks after injury, axon regeneration was almost completely blocked in *Cgas* or *Sting* KO mice but not in *Mavs* KO mice (Figures 4E and 4F). RGC survival was comparable among all groups (Figure S4H). None of the KOs alone affected the axon regeneration (Figure 4G).

To test whether STING activation can promote axon regeneration, we directly injected 2′,3′-cGAMP into the mouse eye and performed the optic nerve crush. STING ligand 2′,3′-cGAMP is a cyclic dinucleotide (CDN) produced in mammalian cells, and exogenous 2′,3′-cGAMP can be transported into cells and activate STING. At 2 weeks after injury, 2′,3′-cGAMP stimulated significant axon regeneration (Figure 4H), which was almost completely blocked in *Sting* KO mice but not in *Cgas* or Mavs KO mice (Figure 4I). The synthetic CDN ADU-S100, which is under clinical trials for cancer immunotherapy, also showed a regenerative effect in a dose-dependent manner (Figure S4I). To assess whether neuronal STING is essential for the regeneration induced by cGAMP, we crossed *Vglut2*-cre mice with Credependent SpCas9 mice (*Vglut2*-SpCas9) to express Cas9 in excitatory neurons and injected AAV-sgRNA into the eye to KO STING in RGCs (Figures S4J and S4K). We found that cGAMP-induced regeneration was suppressed in *Vglut2*-SpCas9 mice injected with AAV-sgRNA-*Sting* but not in those injected with AAV-sgRNA-ctrl (Figures S4L and S4M). Thus, neuronal cGAS-STING signaling in RGCs plays a critical role in mediating the axon regeneration induced by *Ptpn2* deletion plus IFNγ.

Axonal IFNγ is locally translated after peripheral axon injury

Since axons spontaneously regenerate after injury in the adult PNS, we wondered how the IFNγ and cGAS-STING pathways are regulated and whether they play any role in the regeneration process. 3 days after sciatic nerve injury in adult WT mice, we examined the level of IFNγ in the DRGs and sciatic nerves (Figure 5A). We performed immunostaining

and found that elevated IFNγ almost exclusively colocalized with axons, but not myelin sheaths labeled with myelin basic protein (MBP) staining in the injured sciatic nerve at 3 h post crush (hpc) and at 3 dpc (Figures 5B and 5C). Western blot showed that the level of IFNγ was high in DRGs and not significantly changed after injury, while IFNγ was weakly detected in the uninjured nerve and evidently increased after injury (Figures 5D and 5E), consistent with immunostaining. Then, we carried out the double-ligation experiment to check whether the IFNγ elevation in the injured axons was due to the axonal transport from either the DRG neuron soma or the axon terminal. We found that IFNγ signal showed up in the proximal ligation site, the interlesional segment and the distal ligation site, without obvious accumulations at the notches (Figure S5A), indicating that axonal transport did not play an essential role in increasing the axonal IFNγ.

To examine whether *Ifng* mRNA was transported to axons before injury, we performed *in situ* hybridization chain reaction (HCR)[56] coupled with Tuj1 immunostaining to detect *Ifng* mRNA in cultured DRG neurons. The result indicated that *Ifng* mRNA colocalized with the DRG neurites (Figure S5B). Then, we further asked if *Ifng* mRNA was also stored in peripheral axons of DRG neuron *in vivo*. For *in vivo* experiment, we used RNAScope to amplify the signal of *Ifng* mRNA on sections of sciatic nerves. Consistent with the *in vitro* experiment, *Ifng* mRNA was detected in axons of sciatic nerves (Figure 5F). To confirm whether the *Ifng* mRNA was translated in axons, we utilized an *ex vivo* model to test the effect of translation inhibition. Sciatic nerve was first crushed and cut into segments. The injured nerve segments were then incubated in Dulbecco's modified eagle medium (DMEM) with a translation inhibitor, anisomycin for 3 h. IFNγ immunostaining indicated that anisomycin treatment reduced over 50% of the IFNγ signal (Figures 5G and 5H). To exclude the possibility that axonal IFNγ is derived from non-neuronal cells within the sciatic nerve, we delivered AAV9-shRNA-*Ifng* intrathecally to knock down *Ifng* in DRG neurons. As shown by the immunostaining of IFNγ in the cross sections of the injured sciatic nerves, this knockdown method effectively infected DRG neurons and deceased the axonal level of IFNγ by over 60% (Figures 5I and S5C). In dramatic contrast to what we found in the PNS, we did not detect the elevation of axonal IFNγ in either the central spinal branches of the DRG neurons after spinal cord injury (Figures 5J and S5D) or in the axons of the optic nerve after injury (Figures 5K and S5D), in which Thy1-GFP mice were used to label individual axons. To investigate how the nerve injury triggers the local translation of *Ifng* mRNA, through a candidate approach, we injected compounds or inhibitors into nerves, performed crush and examined IFNγ by immunostaining. Voltage-gated calcium channels (VGCCs) inhibitor CdCl2, calcium chelator EGTA, and mTOR inhibitors suppressed axonal IFNγ (Figures S5E and S5F). Ca^{2+}/calmodulin-dependent protein kinase II (CaMKII), extracellular signal-regulated kinase (ERK) and dual leucine zipper kinase (DLK) inhibitors did not have effect on the IFNγ level (Figures S5E and S5F). Therefore, calcium influx and mTOR signaling were essential for axonal IFNγ translation. Our results indicate that IFNγ is locally translated within the axons upon peripheral axotomy.

Axonal IFNγ is required for peripheral axon regeneration

To examine the function of IFNγ in the regeneration, we delivered AAV9-shRNA-*Ifng* intrathecally to knock down *Ifng* in DRG neurons. At 3 dpc, we evaluated the sensory axon

regeneration by SCG10 staining and observed that AAV-shRNA-*Ifng* partially suppressed spontaneous axon regeneration in comparison with control shRNA (Figures 6A and 6B). Then, we investigated the underlying mechanism. First, the elevation of neither p-STAT3 nor phosphorylated cJun (p-cJun) in injured DRG neurons was affected by *Ifng* knockdown (Figures 6C and 6D), indicating that regeneration inhibition was unlikely mediated by targeting canonical retrograde injury signals.[57] Next, we analyzed a published transcriptomic dataset[4] and found that four ISGs were upregulated at 3 dpc after sciatic nerve axotomy (SNA), but not dorsal column axotomy (DCA) (Figure S6A). To examine whether IFNγ signaling regulates axonal regeneration in a cell-autonomous fashion, we deleted *Ifngr1* from DRG neurons by intrathecal delivery of AAV9-Cre into *Ifngr1* floxed mice (Figure S6B). The efficacy of AAV was demonstrated using the Tomato Cre reporter mouse line, and over 90% of lumbar DRG neurons were infected by AAV (Figure S6C). Although *Ifngr1* KO decreased the expression of some ISGs (Figure S6D), we did not observe obvious differences in the axon regeneration between the AAV-Cre and AAV-GFP groups (Figures S6E and S6F). In the isolated DRG neuron culture, RU.521, a potent and selective inhibitor of cGAS, did not show any effect on the axon elongation, indicating that cGAS in DRG neurons is unlikely to be critical for axon regeneration (Figures S6G and S6H). Then, we assessed whether IFNγ may influence the regeneration locally at the lesion site by injecting IFNGR1 antibody into the sciatic nerve at the time of injury (Figure 6E). The efficacy of the antibody was demonstrated by the suppression of some of the signature ISGs in the injured sciatic nerve (Figure 6F), which also indicated that the released IFNγ from axons triggered the expression of many ISGs in the cells in the injured sciatic nerve. We found that spontaneous regeneration was inhibited by IFNGR1 antibody to a similar degree as by *Ifng*-shRNA, but not by either IgG control or IFNAR1 antibody (Figures 6G and 6H). Our results support the notion that axonal IFNγ stimulates axon regeneration in a non-cell-autonomous manner after sciatic nerve injury.

IFNγ elevates cGAS expression in the injured sciatic nerve to promote axon regeneration

Peripheral axon regeneration is facilitated by different types of cells in the injured nerves,[58,59] and we hypothesized that IFNγ may regulate axon regeneration indirectly by stimulating these non-neuronal cells. From our RGC experiments (Figure 4A), one such candidate molecule is cGAS. Western blotting of the injured sciatic nerve protein samples showed that IFNγ was increased within 3 h, while cGAS was significantly elevated at 12 hpc (Figures 7A–7C). At 3 dpc, we performed immunostaining of the sciatic nerve and found that many cGAS+ cells were observed around and distal to the lesion site (Figure 7D). cGAS did not colocalize with the axonal marker Tuj1 (Figure 7E), but with the hematopoietic cell marker CD45 (Figure 7F) and the Schwann cell marker S100b (Figure 7G). To test whether IFNγ stimulates cGAS expression, we infused the IFNGR1 antibody into the lesioned nerve. Western blot analysis shows that the cGAS level was evidently suppressed but not affected by either control antibody or IFNAR1 antibody infusion (Figures 7H and 7I). The number of cGAS+ cells distal to the lesion site was decreased (Figures S7A and S7B). We also detected pH2A.X in Schwann cells and blood cells after injury (Figure S7C), suggesting that cGAS could be activated by DNA damage. Overall, these results indicated that IFNγ may be secreted or released from injured or degenerating axons

and likely stimulates cGAS expression in the Schwann cells and/or hematopoietic cells in the sciatic nerve.

Next, we examined the role of the cGAS elevation in axon regeneration. We injected RU.521 into the crushed sciatic nerve to suppress cGAS activation within the nerve (Figure 7J). RU.521 administration inhibited axon regeneration by over 40% at 3 dpc (Figures 7K and 7L). Thus, cGAS expression in Schwann cells and/or hematopoietic cells stimulated by axonal IFNγ is essential for the axonal regeneration in the PNS.

Injury-induced cGAMP promotes peripheral regeneration through axonal STING

Next, we hypothesized that cGAS elevation in non-neuronal cells within the sciatic nerve may produce cGAMP and enhance axon regeneration by activating STING. In DRG culture, either cGAMP or DMXAA, a mouse-specific STING ligand, enhanced the axon elongation (Figures 8A and 8B). STING inhibitors decreased the axon growth *in vitro* (Figures 8A and 8B). This result was also confirmed by using *Sting* KO mice (Figures 8C and 8D). The growth effect of cGAMP on DRG culture was completely abolished with *Sting* deletion (Figures 8C and 8D). As control, *Mavs* KO did not show any evident effects with or without cGAMP. Next, we injected H151 into the crushed sciatic nerve to inhibit STING activation within the nerve. H151 administration partially suppressed axon regeneration at 3 dpc (Figures 8E and 8F). As cGAS was mostly elevated in the lesion site and the distal nerve, this immediately raised the question of how cGAMP works to promote the regrowth. By using microfluidic chambers, we cultured DRG neurons with their cell bodies and axons in separate compartments, where compounds could be added to one compartment without affecting the other. We severed axons by vacuum aspiration in the axonal chamber to mimic axotomy. Then, ADU-S100 was added to the axonal compartment or the soma compartment. We found that ADU-S100 treatment on either side enhanced axon elongation (Figures 8G and 8H). LRRC8 volume-regulated anion channels have been identified as cGAMP transporters.[60,61] Adding LRRC8 blocker DCPIB or CBX into DRG culture could inhibit the growth effect induced by cGAMP (Figure S8A), indicating that cGAMP is imported into DRG neurons through these channels. Thus, locally produced $2',3'$-cGAMP could enhance the axon regeneration by activating STING in the axons.

To understand the mechanism of neuronal STING enhancing axon regeneration, we injected cGAS inhibitor RU521 into the injured sciatic nerve to suppress STING activation and performed RNA-seq analysis of DRGs. Comparing with control, several genes related to axon elongation were suppressed by cGAS-STING inhibition, including *Sprr1a* and *Gadd45a*, previously shown as regenerating associated genes, and others (Figure S8B). By doing qPCR, we verified that these genes were indeed upregulated by peripheral nerve injury and suppressed by RU521 injection (Figure S8C). Then, we knocked down each candidate gene in cultured DRG neurons with or without cGAMP treatment. Among them, *Tubb6* knockdown blocked the growth effect of cGAMP (Figure S8D), indicating *Tubb6* could be one of the functional downstream effectors of STING activation. Since *Tubb6* encodes tubulin beta 6, we sought to examine the microtubule dynamics and growth cone morphology with STING agonist treatment (Figure 8I). ADU-S100 increased the growth cone area of DRG axons (Figure 8J), and recruited more EB1-GFP, a marker of growing

microtubules,[62] to growth cones (Figure 8K). By recording the velocity of EB1-GFP comet in the growth cone, we found that ADU-S100 increased the microtubule growth speed (Figures 8L and 8M). Taken together, STING activation regulated transcriptional changes in DRG neurons and the local microtubule dynamics to promote axon regeneration.

To evaluate the functional effect of PTPN2 in PNS injury, we knocked out *Ptpn2* in adult DRG neurons using tamoxifen-inducible Advillin-CreERT2;*Ptpn2 flox* mice and performed sciatic nerve crush. Consistent with the *in vitro* result, *Ptpn2* deletion further promoted peripheral sensory axon regeneration after injury (Figures S8E and S8F). In the pinprick test, *Ptpn2* cKO in DRG neurons accelerated the functional recovery in comparison with control (Figure S8G) and enhanced the reinnervation of the axon terminals into the hindpaw skin shown by GAP43 staining (Figures S8H and S8I). Then we wondered whether *Ptpn2* deletion promoted peripheral axon regeneration through a similar mechanism as in RGCs, and did western blotting of DRGs (Figure S8J). *Ptpn2* cKO enhanced STAT1-cGAS-STING signaling in injured DRGs (Figures S8K and S8L). In addition, we detected pH2A.X staining in *Ptpn2* cKO DRG neurons (Figure S8M), suggesting that cGAS could be activated by DNA damage in *Ptpn2* cKO DRG neurons but not in WT. Consistently, cGAS inhibitor RU.521 suppressed the axon growth of *Ptpn2* cKO neurons but not WT neurons (Figures S8N and S8O). Thus, *Ptpn2* cKO in DRG neurons promoted peripheral regeneration via activating neuronal cGAS-STING pathway.

DISCUSSION

In this study, we propose two different models of how antiviral mechanisms in the nervous system contribute to axon regeneration. First, in the CNS, the activation of the IFNγ-STAT1 pathway promotes axon regeneration through a neuron-autonomous mechanism. This result suggests that retinas control their immune response by multiple layers of inhibition, and the removal or suppression of such inhibitors (e.g., PTPN2) can assist RGC axon regeneration. Second, in the PNS, IFNγ is secreted by injured axons and promotes axon regeneration through a non-cell-autonomous mechanism by upregulating cGAS expression in Schwann cells and blood cells. Finally, cGAS may produce the immunotransmitter $2^{'},3^{'}$-cGAMP, and neuronal STING senses cGAMP to mediate axon regeneration. Collectively, our study shows that different immune responses after CNS and PNS injury mediate the differential axon regeneration outcomes and elucidates how the antiviral mechanism is coordinated to promote axon regeneration.

Upon virus infection, intracellular PRRs sense cytosolic viral DNA or RNA, then trigger the expression of interferons to activate JAK-STAT signaling.[27,28] In our study, we found that neuronal cGAS in the CNS and PNS or non-neuronal cGAS in the PNS could be upregulated by IFNγ-STAT1 signaling and facilitate axon regeneration. Neuronal Ptpn2 deletion leads to DNA damage, cytoplasmic dsDNA accumulation, and subsequently cGAS activation, consistent with previous result that increasing DNA damage in injured DRG neurons promotes axon regeneration.[63]

Early studies have demonstrated that both central and peripheral neurons can synthesize protein locally in axons.[64–66] The proteins from local translation can support axon

regeneration by serving as the building block for axon extension or the retrograde signaling molecule for axotomy. Recently, Kong et al. performed a proteomic study and found that the protein composition in peripheral and central branches of DRG are different.[67] However, it is still unclear whether it is a result of differences in local translation between the central and peripheral axons. In our study, we discovered that IFNγ is synthesized in axons after axotomy and can modify the niche for axon regeneration. Surprisingly, the production of IFNγ only occurs in the peripheral axons, but not in the central axons of DRG. Given the vulnerability of CNS neurons, this unilateral enhancement could be a mechanism to prevent the potential detrimental effect of cell death induced by excessive IFNγ, while also restricting the extent of the environmental injury response. Future experiments should focus on elucidating the mechanism causing such difference.

We observed the secretion of IFNγ from axons after sciatic nerve injury. Although we mainly focused on its function of facilitating axon regeneration, IFNγ in peripheral axons may also play a role in defending against viruses. Consistent with our results, Song et al. found that treating peripheral axons with IFNγ reduced retrograde viral infection of the neuronal cell body.[68] These results suggested that neuroinflammation may be involved in the antipathogen function and axonal regeneration at the same time. After axotomy, IFNγ stimulates cGAS expression in Schwann cells and blood cells to produce cGAMP, which might further increase interferons in the nerve and DRG. Such a feedback loop possibly simultaneously maintains the expression of ISGs to sustain axon regeneration and prevents potential viral spreading. Future studies should look for other downstream ISGs potentially involved in the axon growth, which can further explain the correlation between regeneration and the antiviral process during neuroinflammation, and the potential role of ISGs in the regeneration capacity in different neuron subtypes.[69–71] Our findings also raise possible implications for the loss of the regeneration capacity in CNS neurons and the evolution of pathogen resistance.[72,73]

STAR★METHODS

KEY RESOURCES TABLE

REAGENT or RESOURCE	SOURCE	IDENTIFIER
Antibodies		
Rabbit anti-FITC	Invitrogen	Cat#71–1900; RRID: AB_2533978
Mouse anti-GAPDH	ProteinTech	Cat#60004–1-Ig; RRID: AB_2107436
Mouse anti-Tuj1	BioLegend	Cat#801202; RRID: AB_10063408
Mouse anti-dsDNA	Abcam	Cat#27156; RRID: AB_470907
Chicken anti-Tuj1	Aves Labs	Cat#TUJ; RRID:AB_2313564
Chicken anti-NFH	Aves Labs	Cat#NFH; RRID: AB_2313552
Chicken anti-GFAP	Aves Labs	Cat#GFAP; RRID: AB_2313547
Rabbit anti-Iba1	Wako Chemicals USA	Cat# 019–19741; RRID: AB_839504

REAGENT or RESOURCE	SOURCE	IDENTIFIER
Rabbit anti-Tuj1	BioLegend	Cat#802001; RRID: AB_2564645
Rabbit anti-TurboGFP	Evrogen	Cat#AB513
Rabbit anti-IFNγ	Abcam	Cat#ab9657; RRID: AB_2123314
Rabbit anti-cGAS	Cell Signaling	Cat#31659; RRID: AB_2799008
Rabbit anti-STING	Cell Signaling	Cat#13647; RRID: AB_2732796
Rabbit anti-SCG10	Novus	Cat#NBP1–49461; RRID: AB_10011569
Rat anti-CD45	BioLegend	Cat#103101; RRID: AB_312966
Rabbit anti-S100β	Cell Signaling	Cat#9550; RRID: AB_10949319
Rabbit anti-pSTAT1	Cell Signaling	Cat#9167; RRID: AB_561284
Rabbit anti-STAT1	Cell Signaling	Cat#14994; RRID: AB_2737027
Rabbit anti-pSTAT3	Cell Signaling	Cat#9145; RRID: AB_2491009
Rabbit anti-pH2A.X	Cell Signaling	Cat#9718; RRID: AB_2118009
Rabbit anti-TOMM20	Abcam	Cat#186735; RRID: AB_ 2889972
Mouse control neutralizing antibody	BioXCell	Cat#BE0089; RRID: AB_1107769
Mouse IFNGR1 neutralizing antibody	BioXCell	Cat#BE0029; RRID: AB_1107576
Mouse IFNAR1 neutralizing antibody	BioXCell	Cat#BE0241; RRID: AB_2687723
Goat anti Mouse 488	Invitrogen	Cat#A-11029; RRID: AB_138404
Goat anti Mouse 555	Invitrogen	Cat#A-21424; RRID: AB_141780
Goat anti Mouse Cy5	Invitrogen	Cat#A10524; RRID: AB_2534033
Goat anti Rabbit 488	Invitrogen	Cat#A-11008; RRID: AB_143165
Goat anti Rabbit 555	Invitrogen	Cat#A-21429; RRID: AB_2535850
Goat anti Rabbit Cy5	Invitrogen	Cat#A-10523; RRID: AB_2534032
Goat anti Chicken 488	Invitrogen	Cat#A-11039; RRID: AB_142924
Goat anti Chicken 555	Invitrogen	Cat#A-21437; RRID: AB_2535858
Goat anti Chicken 647	Invitrogen	Cat#A-21449; RRID: AB_2535866
Bacterial and virus strains		
pAAV.hSyn.eGFP.WPRE.bGH	James M. Wilson (unpublished data)	Cat#105539; RRID: Addgene_105539
pAAV.hSyn.HI.eGFP-Cre.WPRE.SV40	Penn Vector	Cat#P1848
pAAV.U6.shRLuc.CMV.EGFP.SV40	Penn Vector	Cat#P1867
pAAV-U6 sgRNA(SapI)_hSyn-GFP-KASH-bGH	Swiech et al.[74]	Cat#60958; RRID: Addgene_60958
Chemicals, peptides, and recombinant proteins		
Cholera Toxin B Subunit, FITC Conjugate	Sigma-Aldrich	Cat#C1655
IFNγ	Prospec	Cat#cyt-358
leptin	Prospec	Cat#cyt-351
insulin	ThermoFisher	Cat#12585014
EGF	Prospec	Cat#cyt-217

REAGENT or RESOURCE	SOURCE	IDENTIFIER
NGF	Prospec	Cat#cyt-579
RU.521	MedChemExpress	Cat#HY-114180
C-176	MedChemExpress	Cat# HY-112906
H-151	MedChemExpress	Cat# HY-112693
2', 3'-cGAMP	MedChemExpress	Cat#HY-100564A
DMXAA	MedChemExpress	Cat# HY-10964
ADU-S100	MedChemExpress	Cat#HY-12885A
CdCl2	Sigma-Aldrich	Cat#202908
Torin1	MedChemExpress	Cat#HY-13003
pp242	MedChemExpress	Cat#HY-10474
Thapsigargin	Sigma-Aldrich	Cat#T9033
EGTA	Sigma-Aldrich	Cat#E3889
KN93	MedChemExpress	Cat# HY-15465
SCH772984	MedChemExpress	Cat# HY-50846
DLK-IN-1	Adooq	Cat#A18676
Anisomycin	Sigma-Aldrich	Cat# A9789
Paraformaldehyde (PFA)	Sigma-Aldrich	Cat#30525–89-4
Optimal Cutting Temperature compound	SAKURA	Cat#4583
Triton X-100	Sigma-Aldrich	Cat#T8787
Normal goat serum	Invitrogen	Cat#50062Z
Neurobasal A	Gibco	Cat#10888022
Neurobasal	Gibco	Cat#21103049
Leibovitz's L-15 medium	Gibco	Cat#21083027
TrypLE	Gibco	Cat#12604021
GlutaMAX	Gibco	Cat#35050061
5-fluoro-2'-deoxyuridine	Sigma	Cat#F0503
B27 supplement	Gibco	Cat#17504044
penicillin-streptomycin	Gibco	Cat#15140122
Fetal bovine serum	HyClone	Cat#SH3007103
DMEM	Gibco	Cat#12800017
Papain	Sigma-Aldrich	Cat#P4762
DMSO	Sigma-Aldrich	Cat#D2650
Sucrose	Invitrogen	Cat#15503022
DAPI	Sigma-Aldrich	Cat#D9542
Collagenase	Roche	Cat#11088858001
Laminin	Gibco	Cat#23017015
PhosSTOP	Roche	Cat#04906837001
cOmplete Tablets	Roche	Cat#05892791001
Critical commercial assays		
Critical commercial assays		
Mouse Neuron Nucleofector Kit	Lonza	Cat#VPG-1001

REAGENT or RESOURCE	SOURCE	IDENTIFIER
HCR 3.0 RNA-FISH Kit	Molecular Instrument	N/A
RNAScope Multiplex Fluorescence V2	ACDBio	Cat#323133
KAPA HiFi HotStart ReadyMix	Roche	Cat#KK2601
SuperScript II Reverse Transcriptase	Invitrogen	Cat#18064014
LightCycler 480 SYBR Green I Master	Roche	Cat#04707516001
Comet assay kit	Abcam	Cat#ab238544
RNAeasy mini Kit	QIAGEN	Cat#74104
Experimental models: Cell lines		
SpCas9 Neuro2a	GeneCopoeia	Cat#SL509
Experimental models: Organisms/strains		
Mouse: Adult C57Bl6/J	Charles River	N/A
Mouse: *Ptpn2* flox	This paper	N/A
Mouse: *Ptpn2*tm1a(EUCOMM)Wtsi	International Mouse Phenotyping Consortium	Cat#: MGI97806
Mouse: *Jak1* flox	This paper	N/A
Mouse: *Stat3* flox	Moh et al.[75]	Cat#:016923; RRID: IMSR_JAX:016923
Mouse: *Mtor* flox	Risson et al.[76]	Cat#:011009; RRID: IMSR_JAX:011009
Mouse: *Ifngr1* flox	Lee et al.[77]	Cat#025394; RRID: IMSR_JAX:025394
Mouse: *Pten/Socs3* flox	Sun et al.[50]	N/A
Mouse: *Advillin-CreER*	Lau et al.[78]	Cat#032027; RRID: IMSR_JAX:032027
Mouse: *Sting* knockout	Jin et al.[79]	Cat#025805; RRID: IMSR_JAX: 025805
Mouse: *Cgas* knockout	Schoggins et al.[80]	Cat#026554; RRID: IMSR_JAX:026554
Mouse: *Mavs* knockout	Sun et al.[81]	Cat#008634; RRID: IMSR_JAX:008634
Mouse: *Vglut2-Cre*	Vong et al.[82]	Cat#028863; RRID: IMSR_JAX: 028863
Mouse: *Rosa26-LSL-Cas9* knockin	Platt et al.[83]	Cat#026175; RRID: IMSR_JAX: 026175
Mouse: *Rosa26-LSL-TMT* knockin	Madisen et al.[84]	Cat#:007905; RRID: IMSR_JAX:007905
Mouse: Thy1-GFP line M	Feng et al.[85]	Cat#007788; RRID: IMSR_JAX:007788
Oligonucleotides		
shRNA and sgRNA sequence: Table S4	This paper	N/A
PCR primers: *Ifit1* forward: GTTCTGCTCTGCTGAAAACCC	This paper	N/A
PCR primers: *Ifit1* reverse: CCTGGTCACCATCAGCATTC	This paper	N/A

REAGENT or RESOURCE	SOURCE	IDENTIFIER
PCR primers: *Ifi204* forward: TTCCACTGAAGATGGGTGGC	This paper	N/A
PCR primers: *Ifi204* reverse: TCTGGGTTGAGTGGCTTTCC	This paper	N/A
PCR primers: Mx2 forward: ACCAGAGTGCAAGTGAGGAGCT	This paper	N/A
PCR primers: *Mx2* reverse: GTACTAGGGCAGTGATGTCCTG	This paper	N/A
PCR primers: *Sprr1a* forward: GCCTGAAGACCTGATCACCA	This paper	N/A
PCR primers: *Sprr1a* reverse: GGTAGCACAAGGCAATGGGA	This paper	N/A
PCR primers: *Gadd45a* forward: CTGCAGAGCAGAAGACCGAA	This paper	N/A
PCR primers: *Gadd45a* reverse: GGGTCTACGTTGAGCAGCTT	This paper	N/A
PCR primers: *Tubb6* forward: AATGGTGCCCTGGTCTAAGC	This paper	N/A
PCR primers: *Tubb6* reverse: CTGGTCTGCTGGGACTGTTC	This paper	N/A
PCR primers: *Apod* forward: GGTGTGGCATGCCTGACTAT	This paper	N/A
PCR primers: *Apod* reverse: GCTCACTGTCAGTTTCTCTCAG	This paper	N/A
PCR primers: *Fst* forward: TGACAATGCCACATACGCCA	This paper	N/A
PCR primers: *Fst* reverse: TTCTTCCGAGATGGAGTTGC	This paper	N/A
PCR primers: *Camk1* reverse: AACTGACCAGGCACAGACG	This paper	N/A
PCR primers: *Camk1* reverse: CCCTAATGTCTTCCGCCTGC	This paper	N/A
Deposited data		
RNA-sequencing data	NIH GEO: GSE215132	https://www.ncbi.nlm.nih.gov/geo/browse/
Software and algorithms		
Image J	https://imagej.nih.gov/ij/	RRID: SCR_002285
Prism 6	https://www.graphpad.com/	N/A
RStudio	https://www.rstudio.com/	N/A
R	https://www.r-project.org/	RRID: SCR_001905

RESOURCE AVAILABILITY

Lead contact

More information or request for reagent and resource sharing should be directed to the corresponding author Kai Liu (kailiu@ust.hk).

Materials availability

This study did not generate new unique reagents.

Data and code availability

All data reported in this paper will be shared by the lead contact upon request. RNA-seq data are publicly available as of the date of publication through GEO repositories as detailed in the key resources table. Accession numbers are listed in the key resources table. This paper does not report original code. Any additional information required to reanalyze the data reported in this paper is available from the lead contact upon request.

EXPERIMENTAL MODEL AND SUBJECT DETAILS

Animals

Wild-type (WT, C57BL/6J, Charles River) mice (7–8 weeks old) of both genders were used. *Ptpn2*-flox mice were generated from *Ptpn2*tm1a(EUCOMM)Wtsi. *Ptpn2*tm1a(EUCOMM)Wtsi are heterozygous mice carrying tm1a alleles generated by the European Conditional Mouse Mutagenesis Program (EUCOMM)/the International Mouse Phenotyping Consortium (IMPC) and they were crossed with Flp mice (gifts from Dr. Jun Xia at The Hong Kong University of Science and Technology) to generate the tm1c conditional ready alleles. Homozygous tm1c mice were used as *Ptpn2*-floxed mice in our experiments. *Pten/Socs3* double-floxed mice were gifts from Dr. Zhigang He (Boston Children's Hospital). *Jak1*-floxed and *Stat3*-floxed mice were gifts from Dr. Zhenguo Wu (Hong Kong University of Science and Technology). *Thy1-GFP* mice were gifts from Dr. Nancy Ip (Hong Kong University of Science and Technology). *Mtor*-floxed, *Ifngr1*-floxed, *Avl-CreER*, *Vglut2-Cre*, *Sting* KO, *Cgas* KO, *Mavs* KO, *Rosa26-LSL-TMT* and *Rosa26-LSL-Cas9* mice were purchased from Jackson Laboratory. *Avl-CreER* mice were crossed with *Ptpn2*-flox mice to produce the conditional knockout mice in DRG neurons. *Pten/ Socs3* double-floxed mice were crossed with *Ptpn2*-floxed mice to generate triple-floxed mice. *Vglut2-Cre* mice were crossed with *LSL-Cas9* mice to induce Cas9 expression specifically in excitatory neurons. Genotypes were confirmed by PCR according to protocols from Jackson Laboratory. Both male and female mice were used for experiments. Experiments were performed in accordance with the guidelines of the Laboratory Animal Facility at the Hong Kong University of Science and Technology.

Primary neuronal culture

In-vitro screening model of axon regeneration are based on DRG electroporation and replating culture. Adult DRGs were cultured and replated according to the protocol described previously.[5] In brief, adult mice were euthanized, and L4-L6 DRGs were dissected from both sides. DRGs were dissociated in 0.5% collagenase for 1.5 hours. Then the medium containing collagenase was replaced by Neurobasal A, and DRGs were gently pipetted 20 times for dissociation. For electroporation, dissociated DRG neurons were transfected by Mouse Neuron Nucleofector Kit in Lonza Nucleofector system using program G103. 6 DRGs and 5 μg plasmid were used for each reaction. Neurobasal-A with 10% B27 supplement was used as the culture medium for DRG neurons.

For replating culture, three days after electroporation, the DRG neurons in primary culture were gently flushed by 20–30 pipetting to be resuspended in the culture medium. Then the cells were seeded in a new plate. After 24 hours, cells were fixed by PFA and then stained by Tuj1 and TurboGFP antibodies. The lengths of the longest axons in each DRG neuron were quantified by the NeuronJ plugin in ImageJ. To test the effect of phosphatase inhibitors in replating culture, respective inhibitors (100nM) were added to culture medium two days before replating and right after replating.

For live imaging, cells were analyzed by using an Elyra 7 microscope with 63x/1.46 oil immersion objective and images were processed with SIM2 by Zeiss Zen Black software. Videos were acquired at 1 s intervals for 2 min under Lattice SIM mode. The experiment was repeated three times for each treatment. The growth cone area, EB1 intensity and movement velocity were quantified. Kymograph was processed and analyzed by KymographClear macro toolset for ImageJ and KymographDirect.

To culture embryonic DRG in the compartmented chamber, embryonic DRGs were dissected from E13.5 pregnant C57BL/6 mouse embryos in Leibovitz's L-15 medium on ice. Tissues were dissociated in TrypLE for 15 min at 37 °C. Dissociated neurons were plated in the microfluidic chamber on cleaned glass coverslips pre-coated with poly-D-lysine and laminin in the density of 100000 cells per chamber with 5 ul culture medium supplemented with GlutaMAX (2mM), B27 (20 ml/l), penicillin-Streptomycin, NGF (50ng/ul) and 5-fluoro-2'-deoxyuridine (10uM) into the somal compartment. After one hour, 200 μl medium was added into both the somal and axonal compartment. To perform in-vitro axotomy, axons in the axonal chamber were removed by a glass pipette connected to an aspirator. Then 150 μl medium was quickly added into the empty compartment. 2 days after vacuum, cells were fixed by 4%PFA and then stained by Tuj1 antibody. The lengths or number of longest axons in each chamber were quantified by ImageJ.

Neuro2A cell line

To test the knockout efficiency of *Sting* sgRNA, Neuro2A cells stably expressing SpCas9 were cultured in a humidified 5%CO2 atmosphere at 37°C using Dulbecco Modified Eagle Medium (DMEM) and supplemented with fetal bovine serum. Cells in 12-well plates were then transfected with 1 μg ctrl or *Sting* sgRNA plasmid by Lipofectamine 3000 at the confluency between 70–80%. The transfection was done according to the manufacturer's protocol. Forty-eight hours after transfection, cell sorting was performed with the BD FACSAria III instrument to isolate mCherry-positive cells. The harvested cells were lysed for the following western blot experiment.

METHOD DETAILS

PTPN2 inhibitor

The small molecule inhibitor of PTPN2 (compound 8) was synthesized as described previously.[43]

AAV construct and packaging

AAV serotype 2/1 was used for CNTF overexpression in the retina. AAV serotype 2/2 was used for shRNA or sgRNA expression in RGCs. AAV serotype 2/9 was used for shRNA expression in DRGs. The virus titer was measured by qPCR. The virus titer was 10^{13} GC/mL for all the experiments.

Optic nerve injury

For all surgeries, mice were anesthetized with a mixture of ketamine (80 mg/kg) and xylazine (10 mg/kg). Meloxicam (1 mg/kg) was treated as an analgesic after surgical operation. The procedures for intravitreous injection and optic nerve injury were conducted as previously described.[36] In brief, the edge of the eyelid was clamped with an artery clamp to expose the conjunctiva. 2 μL of virus, PTPN2 inhibitor (1mM in DMSO as stock solution,1~10 μM diluted in PBS as injection solution) or protein solution (Leptin: 2 μg/ μl, insulin: 2 μg/μl, EGF: 1 μg/μl, bNGF: 1 μg/μl, IFNγ: 0.1 μg/μl, diluted in PBS) was injected into the vitreous body with a Hamilton microsyringe. Eye ointment was applied to the cornea after the operation.

Intraorbital optic nerve injury was performed at 2–4 weeks after virus injection or right after PTPN2 inhibitor or protein solution injection. The optic nerve was exposed through an incision on the conjunctiva and crushed by forceps (Dumont #5; Fine Science Tools) for 2 s at 1–2 mm distal to the optic disk. To label the regenerated axons, 2 μL CTB-FITC (1 μg/μL) was injected into the vitreous body two days before the mice were terminated.

Cortical injection of AAV

AAV-Cre was injected to neonatal *Rosa26-LSL-TMT* or *Ptpn2-flox* mice to induce TMT expression or Ptpn2 conditional knockout. Neonatal mice were first cryoanesthetized and 2 μL virus was injected to sensorimotor cortex by injector attached with a glass pipette. Mice were then placed on a warm pad and then returned to the home cage when they are fully awake. Mice were sacrificed two weeks after injection to check the TMT or *Ptpn2* expression.

Spinal cord injury

The procedure of T8 spinal cord complete crush was described previously.[86] In brief, an incision was made on the muscle over the thoracic vertebrae. Then a laminectomy was performed to expose the dorsal part of the T8 spinal cord. The spinal cord crush was done by Dumont #5 forceps. After surgery, the wounded muscle and skin were sutured. The mice were sacrificed three hours or three days after surgery.

Sciatic nerve injury

To induce *Ptpn2* cKO in *Avl-CreER*;*Ptpn2*-flox mice, tamoxifen (20mg/ml in corn oil) was administered to mice by oral gavage at 100mg/kg for consecutive three days. Sciatic nerve crush was performed two weeks after tamoxifen administration.

To knock down *Ifng* in DRG neurons, the AAV9-ctrl or *Ifng*-shRNA was delivered by intrathecal injection four weeks before sciatic nerve injury. The procedure of sciatic nerve

crush was described previously. In brief, an incision was made on the muscle at the middle thigh. Then the exposed nerve was crushed by Dumont #2 forceps for 20 seconds. For nerve injection of antibodies or compounds, 2 μL ctrl, IFNGR1 or IFNAR1 antibody (5 mg/mL), RU.521 (1 mM), or DMSO vehicle were injected to sciatic nerve right after nerve crush. The mice were sacrificed three days after surgery for assessing axon regeneration.

For double-ligation injury model, sciatic nerves were exposed and ligated by 6–0 surgical sutures for 3 hr. The two ligation sites were placed 1mm apart from each other. Mice were sacrificed and perfused by 4% PFA after ligation.

For the ex-vivo model of sciatic nerve injury, the nerves were crushed and then cut into 3–5mm segments. The injured nerve segments were incubated in DMEM supplemented with 10% FBS and 1% penicillin/streptomycin. Translation was inhibited by 200 μg/ ml anisomycin. After 3 hr incubation, nerve segments were fixed by 4%PFA for 2 hr and then proceeded to frozen section.

Pinprick assay

Mice with sciatic nerve injury were first placed on a wire mesh cage for 10 min to habituate the environment. The lateral half of the plantar surface of the hindpaw was averagely divided into five areas. A 31G needle was gently applied to the five areas one by one without moving the hindpaw. When the animal immediately withdrew or moved the hindpaw away from the wire mesh cage, a positive response was recorded. Each area was tested twice. One or two positive responses were graded as 1 and no response was graded as 0 for the tested area. The pinprick score is the total score of the five areas.

Comet assay

Comet assay was performed according to the manufacturer's protocol. In short, agarose gel was first added on a glass slide to form a base layer. FACS-sorted RGCs were mixed with and then embedded in agarose gel. After treating the cells with lysis buffer and alkaline buffer provided by the kit, the glass slides were placed in the horizontal electrophoresis chamber. TBE buffer was used as electrophoresis solution. Voltage was set to 1 volt/cm for 15 min. The gel was stained by vista green DNA dye for 15 min and imaged.

Immunohistochemistry

Mice were first perfused by PBS and then 4% PFA for 5 min for fixation. Respective tissues were dissected and then post-fixed in 4% PFA for two hours. Fixed tissues were incubated in 30% sucrose overnight and then embedded in optimum cutting temperature (OCT) compound. Frozen sections were then permeabilized with 0.1% Triton X-100, blocked by 4% normal goat serum for 30 min, and incubated by respective primary antibodies overnight. After PBS washing three times, sections were incubated by secondary antibodies for two hours and washed three times again. Images were taken by Leica SP8 confocal microscope.

RNA In situ hybridization

A commercial kit for RNA-FISH, hybridization chain reaction (HCR) 3.0 was used to assess the localization of IFNγ mRNA in cultured neurons. The probe set was designed by the manufacturer and the RNA-FISH assay was performed according to the manufacturer's protocol. In short, cells were fixed by 4% PFA for 10 min. Coverslips were pretreated by hybridization buffer for 30 min and then incubated with 5nM probe in 37 °C overnight. B1 HCR amplifier was used for the amplification step. The Tuj1 staining was performed after amplification. RNA-FISH experiments on tissue sections were performed by using RNAscope Multiplex Fluorescent Reagent Kit v2 according to the manufacturer's protocol. The Tuj1 staining was performed after TSA amplification.

Western blot

DRG, sciatic nerve or cell pellet was first homogenized and lysed in RIPA buffer for 45 minutes. The RIPA buffer consists of 50 mM Tris-HCl at pH 8.0, 150 mM NaCl, 1% Nonidet P-40, 0.5% Na-deoxycholate, 0.5% SDS. The EDTA-free cOmplete ULTRA tablets (Roche) and PhosSTOP Complete Easypack (Roche) was added to the RIPA lysis buffer before use. The tissue lysis was centrifuged at 10,000 G for 15 min. 53 SDS sample buffer [300 mM Tris-HCl buffer, 10% SDS, 5% beta-mercaptoethanol, 50% glycerol, 0.05% bromophenol blue] was mixed with the supernatant and heated to 100°C for 15 minutes. Western blotting was performed according to the standard protocol.

RNA extraction and qPCR

L4-L6 DRGs or sciatic nerves were dissected out, and RNA extraction was performed by RNAeasy mini Kit according to the manufacturer's protocol. qPCR was done by the protocol of LightCycler 480 SYBR Green. Three replicates for each sample were used in each run, and *Gapdh* expression was used as the loading control. Related primers for qPCR were listed in key resources table.

RNA sequencing

For single RGC isolation, 7–8 weeks old WT or ptpn2 KO mice received IFNγ injection and optic nerve injury. 2 days after injury, micro-Ruby (500 nL, 5% wt/vol. Invitrogen) was gently injected into the optic nerve. The mice were sacrificed one day later. The retinas were dissected immediately and digested with 0.5 mg/mL papain for 35 min. Then the fetal bovine serum was added to stop the digestion. After centrifugation and resuspension into Neurobasal A, single RGCs were isolated by mouth-pipetting. With a mouth pipette, micro-Ruby positive RGC was pipetted from the original medium drop into a new drop, repeating several times, 5–10 RGCs from one retina were pipetted into a tube containing lysis buffer as a replicate.

cDNA preparation of isolated RGCs or RNA extraction from DRGs was performed by SMART-Seq2 protocol.[87] In brief, cells were lysed in 0.2% Triton X-100. Oligo-dT and dNTP were added into the lysis buffer, and the buffer was incubated at 72 °C for 3 minutes. SuperScriptTM II reverse transcriptase and TSO primer were used for reverse transcription. KAPA HiFi HotStart ReadyMix and ISPCR primer were used to amplify cDNA for 25 cycles. cDNA was purified from the PCR product by Ampure XP beads.

cDNA was sent to Novogene for Illumina sequencing. Raw reads were first aligned to GRCm38 (mm10) mouse reference genome using STAR,[88] and gene counts were calculated using featureCounts. Differential expression genes (DEGs) were assessed with R package DESeq2.[89] Heatmaps were generated using pheatmap package.

To analyze the previously published dataset,[4] we obtained the fragments per kilobase (FPKM) data of ISGs from their dataset and modified the relative expression data by using bar charts in Figure S6A.

QUANTIFICATION AND STATISTICAL ANALYSIS

For quantification of neurite lengths in DRG culture. Cell were fixed and stained with TurboGFP (phosphatase shRNA library screening) or Tuj1. The lengths of the longest axons in each DRG neuron were quantified by the NeuronJ plugin in ImageJ. For phos-photase screening, 5–10 neurons were quantified for each shRNA. For compound test, 10–20 cells from each mouse and 3 mice were quantified in each group.

To quantify the axon regeneration after sciatic nerve crush, signal intensity from SCG10 immunostaning was measured by ImageJ at different distances from the proximal lesion site. The distance between the lesion site and the column with half the intensity of the lesion site was considered as the regeneration index.

The number of surviving RGCs was determined by whole-mount Tuj1 staining. The retina was gently exposed and dissected and was washed with 1X PBS 3 times in a 24-well plate. After incubation in 4% normal goat serum (NGS) for 30 mins, the retina was incubated with Tuj1 antibody overnight at room temperature. After being washed three times with PBS, the retina was incubated with secondary antibodies for one hour at room temperature. After being washed with PBS, the retina was mounted onto glass slides. The images were taken by a confocal microscope (Zeiss, LSM 880; 63X objective). Twelve images were taken from the peripheral and central regions of each retina. The number of Tuj1+ cells was counted in a blinded fashion.

To quantify the number of regenerating axons, the sections of optic nerves (thickness t=8 μm) were stained with the FITC antibody and imaged under a confocal microscope (Zeiss, LSM 880; 10X objective). Five images were taken for quantification from each optic nerve. The number of regenerated axons at indicated distances from the lesion site was estimated by the following formula: $\sum a_d = \pi r^2 x$, where r is the radius of the nerve at the quantification site, the mm is the nerve width at the quantification site, the t indicates the section thickness (8 μm). Axon numbers were counted in a blinded fashion.

To quantify the cGAS positive cells in injured sciatic nerves, a 100μmX100μm square was drawn on sciatic nerve sections at different distance to the lesion center. All the cells (indicated by DAPI staining) within the square were quantified. Cells in intact sciatic nerve sections stained with cGAS antibody were used as the standard of cGAS negative cells. Four nerves were quantified in each group.

All the statistical tests were performed using GraphPad Prism 6 software. Analysis was performed using the student's t-test when comparing the mean between two independent groups. Analysis was performed using one-way analysis of variance (ANOVA) followed by Dunnett's or Tukey's post-test as indicated for multiple groups. An estimate of variation is indicated by the standard error of the mean (SEM). ** p%0.01, * p%0.05.

Supplementary Material

Refer to Web version on PubMed Central for supplementary material.

ACKNOWLEDGMENTS

REFERENCES

1. Chandran V, Coppola G, Nawabi H, Omura T, Versano R, Huebner EA, Zhang A, Costigan M, Yekkirala A, Barrett L, et al. (2016). A systems-level analysis of the peripheral nerve intrinsic axonal growth program. Neuron 89, 956–970. 10.1016/j.neuron.2016.01.034. [PubMed: 26898779]

2. Neumann S, and Woolf CJ (1999). Regeneration of dorsal column fibers into and beyond the lesion site following adult spinal cord injury. Neuron 23, 83–91. [PubMed: 10402195]

3. Hilton BJ, Husch A, Schaffran B, Lin TC, Burnside ER, Dupraz S, Schelski M, Kim J, Müller JA, Schoch S, et al. (2022). An active vesicle priming machinery suppresses axon regeneration upon adult CNS injury. Neuron 110, 51–69.e7. 10.1016/j.neuron.2021.10.007. [PubMed: 34706221]

4. Palmisano I, Danzi MC, Hutson TH, Zhou L, McLachlan E, Serger E, Shkura K, Srivastava PK, Hervera A, Neill NO, et al. (2019). Epigenomic signatures underpin the axonal regenerative ability of dorsal root ganglia sensory neurons. Nat. Neurosci 22, 1913–1924. 10.1038/s41593-019-0490-4. [PubMed: 31591560]

5. Weng YL, Wang X, An R, Cassin J, Vissers C, Liu Y, Liu Y, Xu T, Wang X, Wong SZH, et al. (2018). Epitranscriptomic m(6)A regulation of axon regeneration in the adult mammalian nervous system. Neuron 97, 313–325.e316. 10.1016/j.neuron.2017.12.036. [PubMed: 29346752]

6. Tedeschi A, Dupraz S, Laskowski CJ, Xue J, Ulas T, Beyer M, Schultze JL, and Bradke F (2016). The calcium channel subunit Alpha2delta2 suppresses axon regeneration in the adult CNS. Neuron 92, 419–434. 10.1016/j.neuron.2016.09.026. [PubMed: 27720483]

7. Yang C, Wang X, Wang J, Wang X, Chen W, Lu N, Siniossoglou S, Yao Z, and Liu K (2020). Rewiring neuronal glycerolipid metabolism determines the extent of axon regeneration. Neuron 105, 276–292.e5. 10.1016/j.neuron.2019.10.009. [PubMed: 31786011]

8. Mahar M, and Cavalli V (2018). Intrinsic mechanisms of neuronal axon regeneration. Nat. Rev. Neurosci 19, 323–337. 10.1038/s41583-018-0001-8. [PubMed: 29666508]

9. Fawcett JW (2020). The struggle to make CNS axons regenerate: why has it been so difficult? Neurochem. Res 45, 144–158. 10.1007/s11064-019-02844-y. [PubMed: 31388931]

10. He Z, and Jin Y (2016). Intrinsic control of axon regeneration. Neuron 90, 437–451. 10.1016/j.neuron.2016.04.022. [PubMed: 27151637]

11. Tedeschi A, and Bradke F (2017). Spatial and temporal arrangement of neuronal intrinsic and extrinsic mechanisms controlling axon regeneration. Curr. Opin. Neurobiol 42, 118–127. 10.1016/j.conb.2016.12.005. [PubMed: 28039763]

12. Silver J, Schwab ME, and Popovich PG (2014). Central nervous system regenerative failure: role of oligodendrocytes, astrocytes, and microglia. Cold Spring Harb. Perspect. Biol 7, a020602. 10.1101/cshperspect.a020602. [PubMed: 25475091]

13. Benowitz LI, and Popovich PG (2011). Inflammation and axon regeneration. Curr. Opin. Neurol 24, 577–583. 10.1097/WCO.0b013e32834c208d. [PubMed: 21968547]

14. Hu Z, Deng N, Liu K, Zhou N, Sun Y, and Zeng W (2020). CNTF-STAT3-IL-6 axis mediates neuroinflammatory cascade across Schwann cell-neuron-microglia. Cell Rep 31, 107657. 10.1016/j.celrep.2020.107657. [PubMed: 32433966]

15. Wang Q, Zhang S, Liu T, Wang H, Liu K, Wang Q, and Zeng W (2018). Sarm1/Myd88–5 regulates neuronal intrinsic immune response to traumatic axonal injuries. Cell Rep 23, 716–724. 10.1016/j.celrep.2018.03.071. [PubMed: 29669278]

16. Ben-Yaakov K, Dagan SY, Segal-Ruder Y, Shalem O, Vuppalanchi D, Willis DE, Yudin D, Rishal I, Rother F, Bader M, et al. (2012). Axonal transcription factors signal retrogradely in lesioned peripheral nerve. EMBO J 31, 1350–1363. 10.1038/emboj.2011.494. [PubMed: 22246183]

17. Qiu J, Cafferty WB, McMahon SB, and Thompson SW (2005). Conditioning injury-induced spinal axon regeneration requires signal transducer and activator of transcription 3 activation. J. Neurosci 25, 1645–1653. 10.1523/JNEUROSCI.3269-04.2005. [PubMed: 15716400]

18. Smith PD, Sun F, Park KK, Cai B, Wang C, Kuwako K, Martinez-Carrasco I, Connolly L, and He Z (2009). SOCS3 deletion promotes optic nerve regeneration in vivo. Neuron 64, 617–623. 10.1016/j.neuron.2009.11.021. [PubMed: 20005819]

19. Sas AR, Carbajal KS, Jerome AD, Menon R, Yoon C, Kalinski AL, Giger RJ, and Segal BM (2020). A new neutrophil subset promotes CNS neuron survival and axon regeneration. Nat. Immunol 21, 1496–1505. 10.1038/s41590-020-00813-0. [PubMed: 33106668]

20. Baldwin KT, Carbajal KS, Segal BM, and Giger RJ (2015). Neuroinflammation triggered by beta-glucan/dectin-1 signaling enables CNS axon regeneration. Proc. Natl. Acad. Sci. USA 112, 2581–2586. 10.1073/pnas.1423221112. [PubMed: 25675510]

21. Yin Y, Cui Q, Li Y, Irwin N, Fischer D, Harvey AR, and Benowitz LI (2003). Macrophage-derived factors stimulate optic nerve regeneration. J. Neurosci 23, 2284–2293. [PubMed: 12657687]

22. Schroder K, Hertzog PJ, Ravasi T, and Hume DA (2004). Interferongamma: an overview of signals, mechanisms and functions. J. Leukoc. Biol 75, 163–189. 10.1189/jlb.0603252. [PubMed: 14525967]

23. Roselli F, Chandrasekar A, and Morganti-Kossmann MC (2018). Interferons in traumatic brain and spinal cord injury: current evidence for translational application. Front. Neurol 9, 458. 10.3389/fneur.2018.00458. [PubMed: 29971040]

24. Warre-Cornish K, Perfect L, Nagy R, Duarte RRR, Reid MJ, Raval P, Mueller A, Evans AL, Couch A, Ghevaert C, et al. (2020). Interferon-gamma signaling in human iPSC-derived neurons recapitulates neurodevelopmental disorder phenotypes. Sci. Adv 6, eaay9506. 10.1126/sciadv.aay9506. [PubMed: 32875100]

25. Yasuda M, Nagappan-Chettiar S, Johnson-Venkatesh EM, and Umemori H (2021). An activity-dependent determinant of synapse elimination in the mammalian brain. Neuron 109, 1333–1349.e6. 10.1016/j.neuron.2021.03.006. [PubMed: 33770504]

26. Filiano AJ, Xu Y, Tustison NJ, Marsh RL, Baker W, Smirnov I, Overall CC, Gadani SP, Turner SD, Weng Z, et al. (2016). Unexpected role of interferon-gamma in regulating neuronal connectivity and social behaviour. Nature 535, 425–429. 10.1038/nature18626. [PubMed: 27409813]

27. Ma F, Li B, Yu Y, Iyer SS, Sun M, and Cheng G (2015). Positive feedback regulation of type I interferon by the interferon-stimulated gene STING. EMBO Rep 16, 202–212. 10.15252/embr.201439366. [PubMed: 25572843]

28. Ma F, Li B, Liu SY, Iyer SS, Yu Y, Wu A, and Cheng G (2015). Positive feedback regulation of type I IFN production by the IFN-inducible DNA sensor cGAS. J. Immunol 194, 1545–1554. 10.4049/jimmunol.1402066. [PubMed: 25609843]

29. Ablasser A, and Chen ZJ (2019). cGAS in action: expanding roles in immunity and inflammation. Science 363, eaat8657. 10.1126/science.aat8657. [PubMed: 30846571]

30. Zhang D, Liu C, Li H, and Jiao J (2020). Deficiency of STING signaling in embryonic cerebral cortex leads to neurogenic abnormalities and autistic-like behaviors. Adv. Sci. (Weinh) 7, 2002117. 10.1002/advs.202002117. [PubMed: 33304758]

31. Donnelly CR, Jiang C, Andriessen AS, Wang K, Wang Z, Ding H, Zhao J, Luo X, Lee MS, Lei YL, et al. (2021). STING controls nociception via type I interferon signalling in sensory neurons. Nature 591, 275–280. 10.1038/s41586-020-03151-1. [PubMed: 33442058]

32. Frey E, Valakh V, Karney-Grobe S, Shi Y, Milbrandt J, and DiAntonio A (2015). An in vitro assay to study induction of the regenerative state in sensory neurons. Exp. Neurol 263, 350–363. 10.1016/j.expneurol.2014.10.012. [PubMed: 25447942]

33. Saijilafu Hur, E.M., Liu, C.M., Jiao, Z., Xu, W.L., and Zhou, F.Q. (2013). PI3K-GSK3 signalling regulates mammalian axon regeneration by inducing the expression of Smad1. Nat. Commun 4, 2690. 10.1038/ncomms3690. [PubMed: 24162165]

34. Fisher D, Xing B, Dill J, Li H, Hoang HH, Zhao Z, Yang XL, Bachoo R, Cannon S, Longo FM, et al. (2011). Leukocyte common antigen-related phosphatase is a functional receptor for chondroitin sulfate proteoglycan axon growth inhibitors. J. Neurosci 31, 14051–14066. 10.1523/JNEUROSCI.1737-11.2011. [PubMed: 21976490]

35. Shen Y, Tenney AP, Busch SA, Horn KP, Cuascut FX, Liu K, He Z, Silver J, and Flanagan JG (2009). PTPsigma is a receptor for chondroitin sulfate proteoglycan, an inhibitor of neural regeneration. Science 326, 592–596. 10.1126/science.1178310. [PubMed: 19833921]

36. Park KK, Liu K, Hu Y, Smith PD, Wang C, Cai B, Xu B, Connolly L, Kramvis I, Sahin M, and He Z (2008). Promoting axon regeneration in the adult CNS by modulation of the PTEN/mTOR pathway. Science 322, 963–966. [PubMed: 18988856]

37. Zhang ZY (2017). Drugging the undruggable: therapeutic potential of targeting protein tyrosine phosphatases. Acc. Chem. Res 50, 122–129. 10.1021/acs.accounts.6b00537. [PubMed: 27977138]

38. He R, Wang J, Yu ZH, Zhang RY, Liu S, Wu L, and Zhang ZY (2016). Inhibition of low molecular weight protein tyrosine phosphatase by an induced-fit mechanism. J. Med. Chem 59, 9094–9106. 10.1021/acs.jmedchem.6b00993. [PubMed: 27676368]

39. Zeng LF, Zhang RY, Yu ZH, Li S, Wu L, Gunawan AM, Lane BS, Mali RS, Li X, Chan RJ, et al. (2014). Therapeutic potential of targeting the oncogenic SHP2 phosphatase. J. Med. Chem 57, 6594–6609. 10.1021/jm5006176. [PubMed: 25003231]

40. Zeng LF, Zhang RY, Bai Y, Wu L, Gunawan AM, and Zhang ZY (2014). Hydroxyindole carboxylic acid-based inhibitors for receptor-type protein tyrosine protein phosphatase beta. Antioxid. Redox Signal 20, 2130–2140. 10.1089/ars.2013.5463. [PubMed: 24180557]

41. He Y, Liu S, Menon A, Stanford S, Oppong E, Gunawan AM, Wu L, Wu DJ, Barrios AM, Bottini N, et al. (2013). A potent and selective small-molecule inhibitor for the lymphoid-specific tyrosine phosphatase (LYP), a target associated with autoimmune diseases. J. Med. Chem 56, 4990–5008. 10.1021/jm400248c. [PubMed: 23713581]

42. Zhang S, Liu S, Tao R, Wei D, Chen L, Shen W, Yu ZH, Wang L, Jones DR, Dong XC, and Zhang ZY (2012). A highly selective and potent PTP-MEG2 inhibitor with therapeutic potential for type 2 diabetes. J. Am. Chem. Soc 134, 18116–18124. 10.1021/ja308212y. [PubMed: 23075115]

43. Zhang S, Chen L, Luo Y, Gunawan A, Lawrence DS, and Zhang ZY (2009). Acquisition of a potent and selective TC-PTP inhibitor via a stepwise fluorophore-tagged combinatorial synthesis and screening strategy. J. Am. Chem. Soc 131, 13072–13079. 10.1021/ja903733z. [PubMed: 19737019]

44. Xie L, Lee SY, Andersen JN, Waters S, Shen K, Guo XL, Moller NP, Olefsky JM, Lawrence DS, and Zhang ZY (2003). Cellular effects of small molecule PTP1B inhibitors on insulin signaling. Biochemistry 42, 12792–12804. 10.1021/bi035238p. [PubMed: 14596593]

45. Schoggins JW (2019). Interferon-stimulated genes: what do they all do? Annu. Rev. Virol 6, 567–584. 10.1146/annurev-virology-092818-015756. [PubMed: 31283436]

46. Hubel P, Urban C, Bergant V, Schneider WM, Knauer B, Stukalov A, Scaturro P, Mann A, Brunotte L, Hoffmann HH, et al. (2019). A protein-interaction network of interferon-stimulated

genes extends the innate immune system landscape. Nat. Immunol 20, 493–502. 10.1038/
s41590-019-0323-3. [PubMed: 30833792]

47. Schneider WM, Chevillotte MD, and Rice CM (2014). Interferon-stimulated genes: a complex web
of host defenses. Annu. Rev. Immunol 32, 513–545. 10.1146/annurev-immunol-032713-120231.
[PubMed: 24555472]

48. Bei F, Lee HHC, Liu X, Gunner G, Jin H, Ma L, Wang C, Hou L, Hensch TK, Frank E, et al.
(2016). Restoration of visual function by enhancing conduction in regenerated axons. Cell 164,
219–232. 10.1016/j.cell.2015.11.036. [PubMed: 26771493]

49. Li S, He Q, Wang H, Tang X, Ho KW, Gao X, Zhang Q, Shen Y, Cheung A, Wong F, et
al. (2015). Injured adult retinal axons with Pten and Socs3 co-deletion reform active synapses
with suprachiasmatic neurons. Neurobiol. Dis 73, 366–376. 10.1016/j.nbd.2014.09.019. [PubMed:
25448764]

50. Sun F, Park KK, Belin S, Wang D, Lu T, Chen G, Zhang K, Yeung C, Feng G, Yankner BA, and He
Z (2011). Sustained axon regeneration induced by co-deletion of PTEN and SOCS3. Nature 480,
372–375. 10.1038/nature10594. [PubMed: 22056987]

51. Zhu W, Mustelin T, and David M (2002). Arginine methylation of STAT1 regulates its
dephosphorylation by T cell protein tyrosine phosphatase. J. Biol. Chem 277, 35787–35790.
10.1074/jbc.C200346200. [PubMed: 12171910]

52. ten Hoeve J, de Jesus Ibarra-Sanchez M, Fu Y, Zhu W, Tremblay M, David M, and Shuai K (2002).
Identification of a nuclear Stat1 protein tyrosine phosphatase. Mol. Cell. Biol 22, 5662–5668.
10.1128/MCB.22.16.5662-5668.2002. [PubMed: 12138178]

53. Dalkara D, Kolstad KD, Caporale N, Visel M, Klimczak RR, Schaffer DV, and Flannery JG (2009).
Inner limiting membrane barriers to AAV-mediated retinal transduction from the vitreous. Mol.
Ther 17, 2096–2102. 10.1038/mt.2009.181. [PubMed: 19672248]

54. Xia T, Yi X-M, Wu X, Shang J, and Shu H-B (2019). PTPN1/2-mediated dephosphorylation of
MITA/STING promotes its 20S proteasomal degradation and attenuates innate antiviral response.
Proc. Natl. Acad. Sci. USA 116, 20063–20069. [PubMed: 31527250]

55. Li T, and Chen ZJ (2018). The cGAS-cGAMP-STING pathway connects DNA damage to
inflammation, senescence, and cancer. J. Exp. Med 215, 1287–1299. 10.1084/jem.20180139.
[PubMed: 29622565]

56. Choi HM, Calvert CR, Husain N, Huss D, Barsi JC, Deverman BE, Hunter RC, Kato M, Lee SM,
Abelin AC, et al. (2016). Mapping a multiplexed zoo of mRNA expression. Development 143,
3632–3637. 10.1242/dev.140137. [PubMed: 27702788]

57. Shin JE, Cho Y, Beirowski B, Milbrandt J, Cavalli V, and DiAntonio A (2012). Dual leucine zipper
kinase is required for retrograde injury signaling and axonal regeneration. Neuron 74, 1015–1022.
10.1016/j.neuron.2012.04.028. [PubMed: 22726832]

58. Kalinski AL, Yoon C, Huffman LD, Duncker PC, Kohen R, Passino R, Hafner H, Johnson C,
Kawaguchi R, Carbajal KS, et al. (2020). Analysis of the immune response to sciatic nerve
injury identifies efferocytosis as a key mechanism of nerve debridement. eLife 9, e60223. 10.7554/
eLife.60223. [PubMed: 33263277]

59. Cattin AL, and Lloyd AC (2016). The multicellular complexity of peripheral nerve regeneration.
Curr. Opin. Neurobiol 39, 38–46. 10.1016/j.conb.2016.04.005. [PubMed: 27128880]

60. Lahey LJ, Mardjuki RE, Wen X, Hess GT, Ritchie C, Carozza JA, Bö hnert, V., Maduke, M.,
Bassik, M.C., and Li, L. (2020). LRRC8A: C/E heteromeric channels are ubiquitous transporters
of cGAMP. Mol. Cell 80, 578–591.e5. [PubMed: 33171122]

61. Zhou C, Chen X, Planells-Cases R, Chu J, Wang L, Cao L, Li Z, Ló pez-Cayuqueo, K.I., Xie, Y.,
and Ye, S. (2020). Transfer of cGAMP into bystander cells via LRRC8 volume-regulated anion
channels augments STING-mediated interferon responses and anti-viral immunity. Immunity 52,
767–781.e6. [PubMed: 32277911]

62. Mimori-Kiyosue Y, Shiina N, and Tsukita S (2000). The dynamic behavior of the APC-
binding protein EB1 on the distal ends of microtubules. Curr. Biol 10, 865–868. 10.1016/
s0960-9822(00)00600-x. [PubMed: 10899006]

63. Cheng YC, Snavely A, Barrett LB, Zhang X, Herman C, Frost DJ, Riva P, Tochitsky I, Kawaguchi
R, Singh B, et al. (2021). Topoisomerase I inhibition and peripheral nerve injury induce DNA

breaks and ATF3-associated axon regeneration in sensory neurons. Cell Rep 36, 109666. 10.1016/j.celrep.2021.109666. [PubMed: 34496254]

64. Holt CE, Martin KC, and Schuman EM (2019). Local translation in neurons: visualization and function. Nat. Struct. Mol. Biol 26, 557–566. 10.1038/s41594-019-0263-5. [PubMed: 31270476]

65. Kar AN, Lee SJ, and Twiss JL (2018). Expanding axonal transcriptome brings new functions for axonally synthesized proteins in health and disease. Neuroscientist 24, 111–129. 10.1177/1073858417712668. [PubMed: 28593814]

66. Terenzio M, Schiavo G, and Fainzilber M (2017). Compartmentalized signaling in neurons: From cell biology to neuroscience. Neuron 96, 667–679. 10.1016/j.neuron.2017.10.015. [PubMed: 29096079]

67. Kong G, Zhou L, Serger E, Palmisano I, De Virgiliis F, Hutson TH, McLachlan E, Freiwald A, La Montanara P, Shkura K, et al. (2020). AMPK controls the axonal regenerative ability of dorsal root ganglia sensory neurons after spinal cord injury. Nat. Metab 2, 918–933. 10.1038/s42255-020-0252-3. [PubMed: 32778834]

68. Song R, Koyuncu OO, Greco TM, Diner BA, Cristea IM, and Enquist LW (2016). Two modes of the axonal interferon response limit alphaherpesvirus neuroinvasion. mBio 7 e02145–e02115. 10.1128/mBio.02145-15.

69. Tran NM, Shekhar K, Whitney IE, Jacobi A, Benhar I, Hong G, Yan W, Adiconis X, Arnold ME, Lee JM, et al. (2019). Single-cell profiles of retinal ganglion cells differing in resilience to injury reveal neuroprotective genes. Neuron 104, 1039–1055.e12. 10.1016/j.neuron.2019.11.006. [PubMed: 31784286]

70. Bray ER, Yungher BJ, Levay K, Ribeiro M, Dvoryanchikov G, Ayupe AC, Thakor K, Marks V, Randolph M, Danzi MC, et al. (2019). Thrombospondin-1 mediates axon regeneration in retinal ganglion cells. Neuron 103, 642–657.e7. 10.1016/j.neuron.2019.05.044. [PubMed: 31255486]

71. Duan X, Qiao M, Bei F, Kim IJ, He Z, and Sanes JR (2015). Subtype-Specific Regeneration of Retinal Ganglion Cells following axotomy: effects of osteopontin and mTOR signaling. Neuron 85, 1244–1256. 10.1016/j.neuron.2015.02.017. [PubMed: 25754821]

72. Blackshaw S (2022). Why has the ability to regenerate following CNS injury been repeatedly lost Over the course of evolution? Front. Neurosci 16, 831062. 10.3389/fnins.2022.831062. [PubMed: 35185460]

73. Wu X, Dao Thi VL, Huang Y, Billerbeck E, Saha D, Hoffmann HH, Wang Y, Silva LAV, Sarbanes S, Sun T, et al. (2018). Intrinsic immunity shapes viral resistance of stem cells. Cell 172, 423–438.e25. 10.1016/j.cell.2017.11.018. [PubMed: 29249360]

74. Swiech L, Heidenreich M, Banerjee A, Habib N, Li Y, Trombetta J, Sur M, and Zhang F (2015). In vivo interrogation of gene function in the mammalian brain using CRISPR-Cas9. Nat. Biotechnol 33, 102–106. 10.1038/nbt.3055. [PubMed: 25326897]

75. Moh A, Iwamoto Y, Chai GX, Zhang SS, Kano A, Yang DD, Zhang W, Wang J, Jacoby JJ, Gao B, et al. (2007). Role of STAT3 in liver regeneration: survival, DNA synthesis, inflammatory reaction and liver mass recovery. Lab. Invest 87, 1018–1028. 10.1038/labinvest.3700630. [PubMed: 17660847]

76. Risson V, Mazelin L, Roceri M, Sanchez H, Moncollin V, Corneloup C, Richard-Bulteau H, Vignaud A, Baas D, Defour A, et al. (2009). Muscle inactivation of mTOR causes metabolic and dystrophin defects leading to severe myopathy. J. Cell Biol 187, 859–874. 10.1083/jcb.200903131. [PubMed: 20008564]

77. Lee SH, Carrero JA, Uppaluri R, White JM, Archambault JM, Lai KS, Chan SR, Sheehan KC, Unanue ER, and Schreiber RD (2013). Identifying the initiating events of anti-Listeria responses using mice with conditional loss of IFN-gamma receptor subunit 1 (IFNGR1). J. Immunol 191, 4223–4234. 10.4049/jimmunol.1300910. [PubMed: 24048899]

78. Lau J, Minett MS, Zhao J, Dennehy U, Wang F, Wood JN, and Bogdanov YD (2011). Temporal control of gene deletion in sensory ganglia using a tamoxifen-inducible Advillin-Cre-ERT2 recombinase mouse. Mol. Pain 7, 100. 10.1186/1744-8069-7-100. [PubMed: 22188729]

79. Jin L, Hill KK, Filak H, Mogan J, Knowles H, Zhang B, Perraud AL, Cambier JC, and Lenz LL (2011). MPYS is required for IFN response factor 3 activation and type I IFN production in

the response of cultured phagocytes to bacterial second messengers cyclic-di-AMP and cyclic-di-GMP. J. Immunol 187, 2595–2601. 10.4049/jimmunol.1100088. [PubMed: 21813776]

80. Schoggins JW, MacDuff DA, Imanaka N, Gainey MD, Shrestha B, Eitson JL, Mar KB, Richardson RB, Ratushny AV, Litvak V, et al. (2014). Pan-viral specificity of IFN-induced genes reveals new roles for cGAS in innate immunity. Nature 505, 691–695. 10.1038/nature12862. [PubMed: 24284630]

81. Sun Q, Sun L, Liu HH, Chen X, Seth RB, Forman J, and Chen ZJ (2006). The specific and essential role of MAVS in antiviral innate immune responses. Immunity 24, 633–642. 10.1016/j.immuni.2006.04.004. [PubMed: 16713980]

82. Vong L, Ye C, Yang Z, Choi B, Chua S Jr., and Lowell BB (2011). Leptin action on GABAergic neurons prevents obesity and reduces inhibitory tone to POMC neurons. Neuron 71, 142–154. 10.1016/j.neuron.2011.05.028. [PubMed: 21745644]

83. Platt RJ, Chen S, Zhou Y, Yim MJ, Swiech L, Kempton HR, Dahlman JE, Parnas O, Eisenhaure TM, Jovanovic M, et al. (2014). CRISPR-Cas9 knockin mice for genome editing and cancer modeling. Cell 159, 440–455. 10.1016/j.cell.2014.09.014. [PubMed: 25263330]

84. Madisen L, Zwingman TA, Sunkin SM, Oh SW, Zariwala HA, Gu H, Ng LL, Palmiter RD, Hawrylycz MJ, Jones AR, et al. (2010). A robust and high-throughput Cre reporting and characterization system for the whole mouse brain. Nat. Neurosci 13, 133–140. 10.1038/nn.2467. [PubMed: 20023653]

85. Feng G, Mellor RH, Bernstein M, Keller-Peck C, Nguyen QT, Wallace M, Nerbonne JM, Lichtman JW, and Sanes JR (2000). Imaging neuronal subsets in transgenic mice expressing multiple spectral variants of GFP. Neuron 28, 41–51. 10.1016/s0896-6273(00)00084-2. [PubMed: 11086982]

86. Liu K, Lu Y, Lee JK, Samara R, Willenberg R, Sears-Kraxberger I, Tedeschi A, Park KK, Jin D, Cai B, et al. (2010). PTEN deletion enhances the regenerative ability of adult corticospinal neurons. Nat. Neurosci 13, 1075–1081. 10.1038/nn.2603. [PubMed: 20694004]

87. Picelli S, Faridani OR, Björklund AK, Winberg G, Sagasser S, and Sandberg R (2014). Full-length RNA-seq from single cells using Smart-seq2. Nat. Protoc 9, 171–181. 10.1038/nprot.2014.006. [PubMed: 24385147]

88. Dobin A, Davis CA, Schlesinger F, Drenkow J, Zaleski C, Jha S, Batut P, Chaisson M, and Gingeras TR (2013). STAR: ultrafast universal RNA-seq aligner. Bioinformatics 29, 15–21. 10.1093/bioinformatics/bts635. [PubMed: 23104886]

89. Love MI, Huber W, and Anders S (2014). Moderated estimation of fold change and dispersion for RNA-seq data with DESeq2. Genome Biol 15, 550. 10.1186/s13059-014-0550-8. [PubMed: 25516281]

Highlights

- Neuronal *Ptpn2* deletion amplifies the IFNγ response to promote CNS axon regeneration

- The cGAS-STING pathway is the functional downstream of IFNγ

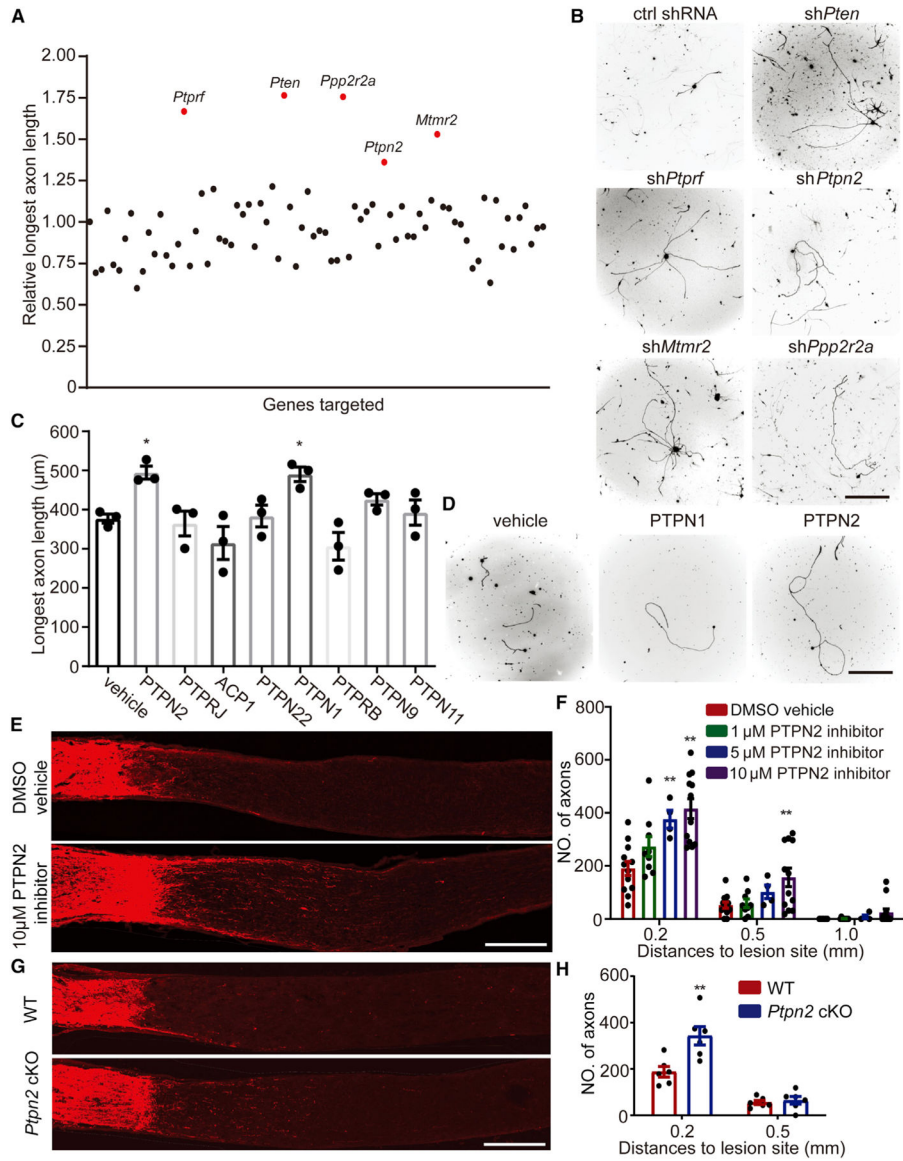- Injured DRG axons release IFNγ that elevates cGAS in Schwann cells and blood cells

Figure 1. Functional screening identifies Ptpn2 as a suppressor of axon regeneration

(A) Quantification of *in vitro* screening on shRNAs of mouse phosphatases.

(B) Sample images of replated neurons from respective shRNA groups with Tuj1 staining. Scale bars, 400 μm.

(C) Quantification of *in vitro* screening on inhibitors of mouse phosphatases. ANOVA followed by Dunnett's test, n = 3 mice.

(D) Sample images of replated neurons from respective treatment groups with Tuj1 staining. Scale bars, 400 μm.

(E) Sections of optic nerves with cholera toxin B subunit (CTB) labeling from WT mice at 2 weeks post-injury (WPI). Scale bars, 200 μm.

(F) Number of regenerating axons at indicated distances from the lesion site. ANOVA followed by Tukey's test, n = 4–12 mice.

(G) Sections of optic nerves from WT or *Ptpn2* floxed mice at 2 WPI. The *Ptpn2* conditional knockout (cKO) was induced by intravitreal injection of AAV-Cre. Scale bars, 200 μm.

(H) Number of regenerating axons at different distances from the lesion site. ANOVA followed by Bonferroni's test, n = 6 mice. Mean ± SEM; *p < 0.05, **p < 0.01.
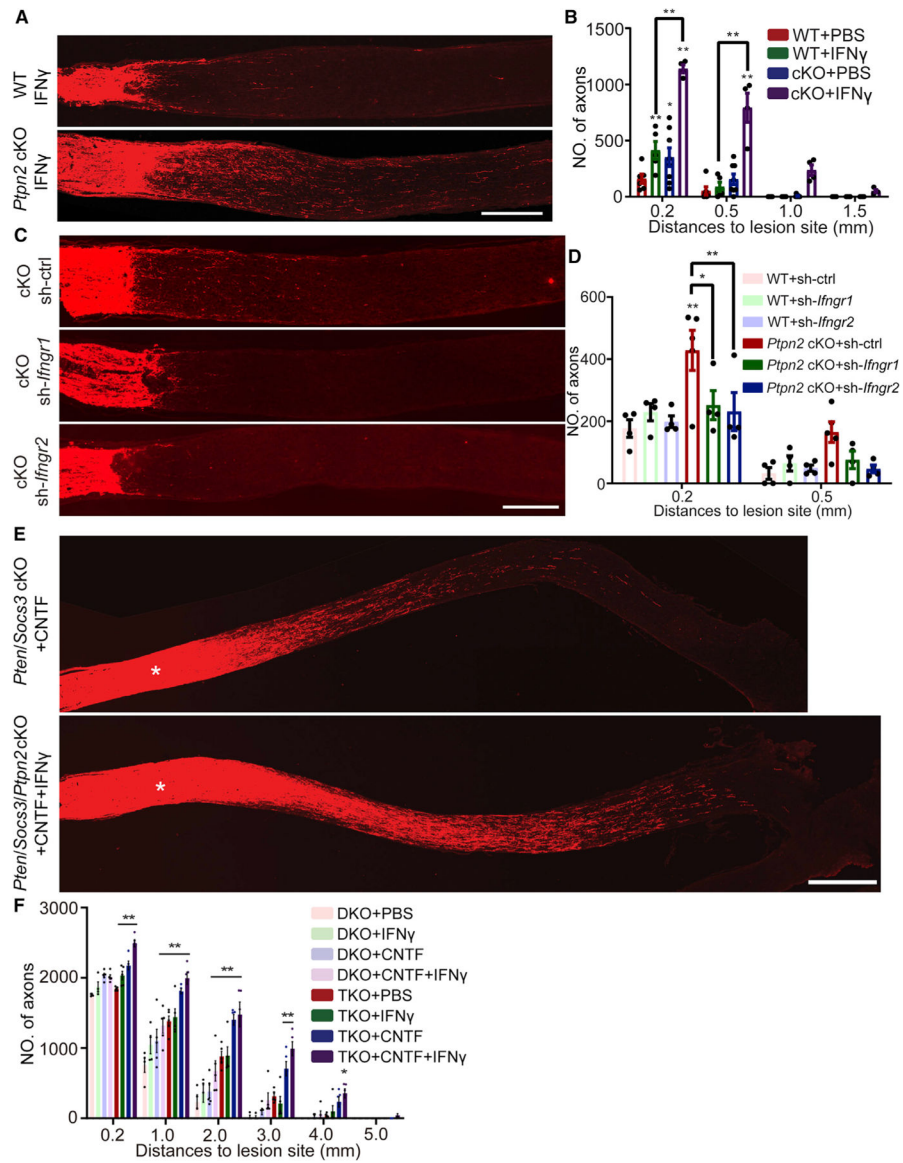
See also Figure S1.

Figure 2. *Ptpn2* deletion effect is boosted by IFNγ and synergizes with *Pten/Socs3* codeletion for long-distance axon regeneration

(A) Sections of optic nerves from WT or *Ptpn2* cKO mice with IFNγ treatment. Scale bars, 200 μm.

(B) Number of regenerating axons at indicated distances distal to the lesion site. ANOVA followed by Tukey's test, n = 4–8 mice.

(C) Sections of optic nerves from *Ptpn2* cKO mice with AAV-sh-Ctrl. Sh-*Ifngr1* or sh-*Ifngr2*. Scale bars, 200 μm.

(D) Number of regenerating axons at indicated distances distal to the lesion site. ANOVA followed by Tukey's test, n = 4–5 mice.

(E) Section of optic nerves from *Pten; Socs3* double-floxed mice or *Pten; Socs3; Ptpn2* triple-floxed mice at 2WPI. The vitreous body was injected with AAV-Cre combined with AAV-CNTF. IFNγ or PBS was injected into the vitreous body immediately after optic nerve injury. Asterisks indicate the lesion site. Scale bars, 500 μm.

(F) Quantification of regenerating axons at indicated distances from the lesion site. ANOVA followed by Bonferroni's test, n = 4–5 mice. Mean ± SEM; *p < 0.05, **p < 0.01.
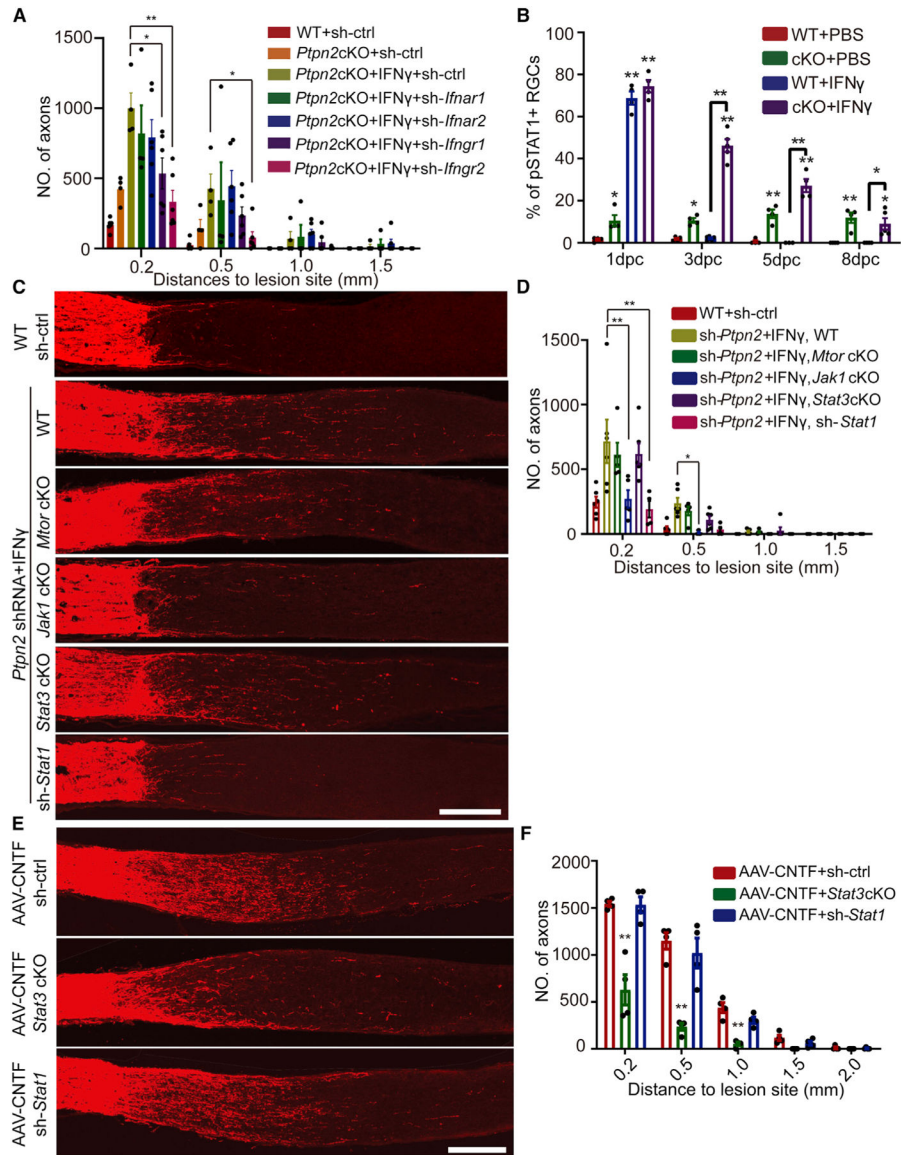
See also Figure S2.

Figure 3. Neuronal *Ptpn2* deletion sustains IFNγ-IFNGR-Stat1 signaling to promote axon regeneration in CNS

(A) Number of regenerating axons at indicated distances distal to the lesion site, ANOVA followed by Tukey's test, n = 4–6 mice.

(B) Quantification of the percentage of p-STAT1+ RGCs at indicated time points after injury in Figure S3E. ANOVA followed by Bonferroni's test. n = 3–5 mice.

(C) Sections of optic nerves from WT, *Mtor* floxed, *Jak1* floxed, or *Stat3* floxed mice at 2WPI. The vitreous body was injected with AAV-Cre or AAV-sh-*Stat1* combined with AAV-sh-*Ptpn2* plus IFNγ. Scale bar, 200 μm.

(D) Number of regenerating axons at indicated distances from the lesion site. ANOVA followed by Tukey's test, n = 4–6 mice.

(E) Sections of optic nerves from WT or *Stat3* floxed mice at 2WPI. The vitreous body was injected with AAV-Cre, AAV-sh-ctrl or AAV-sh-*Stat1* combined with AAV-CNTF. Scale bar, 200 μm.

(F) Quantification of regenerating axons at indicated distances distal to the lesion site. ANOVA followed by Tukey's test, n = 4 mice. Mean ± SEM; *p < 0.05, **p < 0.01. See also Figure S3.
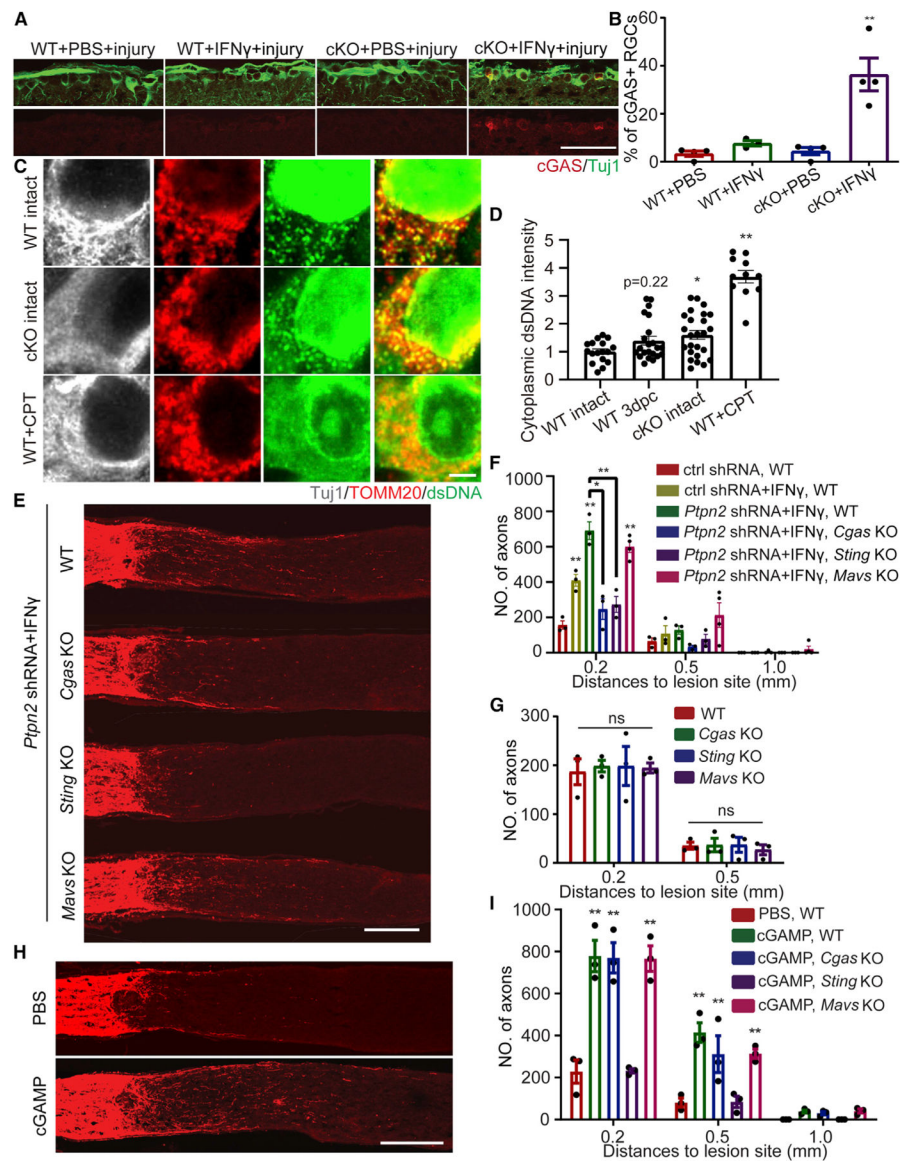
Figure 4. cGAS-STING cytosolic DNA sensing pathway mediates axon regeneration induced by IFNγ

(A) Retinal sections from WT or *Ptpn2* cKO mice with PBS or IFNγ treatment. The samples were collected 2 dpc and stained for Tuj1 (green), and cGAS (red). Scale bar, 50 μm.

(B) Quantification of the percentage of cGAS+ RGCs in (A). ANOVA followed by Dunnett's test. n = 3–4 mice.

(C) Retinal sections from WT intact, cKO intact or WT+CPT mice stained with dsDNA (green), TOMM20 (red), and Tuj1 (gray). Scale bar, 2 μm.

(D) Quantification of relative cytoplasmic DNA intensity from (E). ANOVA followed by Dunnett's test. n = 11–25 cells.

(E) Sections of optic nerves from WT, *Cgas* KO, *Sting* KO, or *Mavs* KO mice at 2WPI. The vitreous body was injected with AAV-sh-*Ptpn2* plus IFNγ. Scale bars, 200 μm.

(F) Number of regenerating axons at indicated distances from the lesion site. ANOVA followed by Tukey's test, n = 3–4 mice.

(G) Quantification of regenerating axons in WT, Cgas KO, Sting KO, or Mavs KO mice. ANOVA followed by Tukey's test, n = 3 mice.

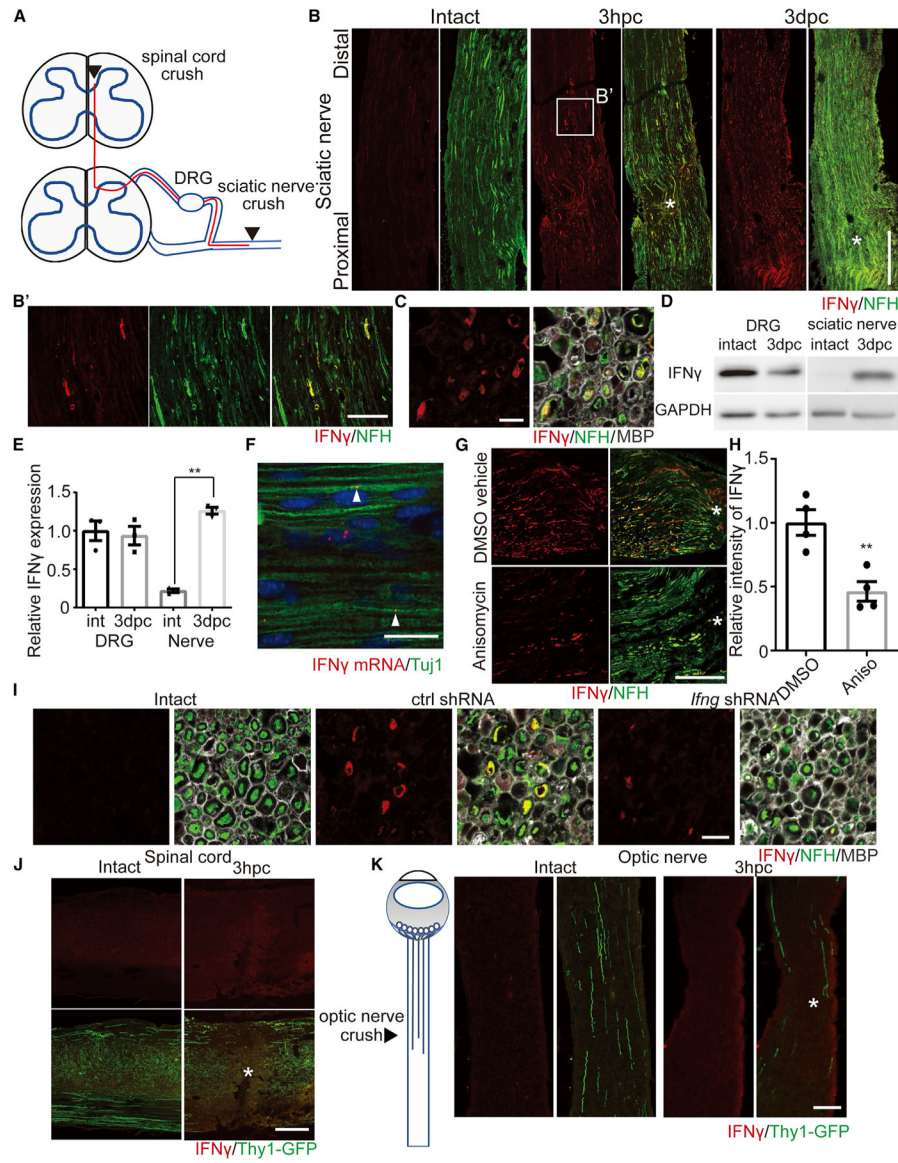(H) Sections of optic nerves from WT mice at 2 WPI, with PBS or 25-mM cGAMP treatment. Scale bar, 200 μm.

(I) Number of regenerating axons at indicated distances from the lesion site. ANOVA followed by Tukey's test, n = 3 mice. Mean ± SEM; *p < 0.05, **p < 0.01.

See also Figure S4.

Figure 5. Axonal IFNγ is locally translated upon axotomy in PNS but not in CNS

(A) A diagram shows the method of sciatic nerve injury and spinal cord injury. Arrowhead labels the location of the lesion site.

(B) Longitude sections of sciatic nerves from WT animals at different time points (intact, 3 hpc and 3 dpc) after injury, stained with IFNγ (red) and NFH (green) antibodies. Scale bars, 200 μm. Zoomed-in images of the 3 hpc sciatic nerve section from (B) are shown in (B′). Scale bars, 50 μm. Asterisks indicate the lesion site.

(C) Cross sections of sciatic nerves from WT animal at 3 dpc, stained with IFNγ (red), MBP (white), and NFH (green) antibodies. Scale bars, 10 μm.

(D) Validation of IFNγ expression in DRG or sciatic nerve lysate by western blot.

(E) Quantification of IFNγ expression in (D). ANOVA followed by Tukey's test, n = 3 mice.

(F) Representative images of the longitude section of an intact sciatic nerve. IFNγ mRNA (red) was stained by *in situ* hybridization and Tuj1 protein was stained by the antibody. Arrowheads indicate the axonal IFNγ mRNA. Scale bar, 20 μm.

(G) Sections of injured nerve segments after 4 h DMEM incubation with control or anisomycin, stained with IFNγ (red) and NFH (green). Asterisks indicate the lesion site. Scale bar, 100 μm.

(H) Quantification of the relative intensity of IFNγ in (G). Student's t test, n = 4 nerves.

(I) Cross sections of injured sciatic nerves from WT animals with intrathecal injection of AAV-ctrl or *Ifng*-shRNA were stained with IFNγ (red), MBP (gray), and NFH (green). Scale bars, 10 μm.

(J) Sections of the spinal cord from Thy1-GFP animal before injury or at 3 hpc after injury, stained with IFNγ (red) and GFP (green) antibodies. Asterisk labels the location of the lesion site. Scale bar, 400 μm.

(K) A diagram shows the method of optic nerve injury. Confocal images are sections of the optic nerve from Thy1-GFP animal before injury or at 3 hpc after injury, stained with IFNγ (red) and GFP (green) antibodies. Asterisk labels the location of the lesion site. Scale bar, 50 μm.

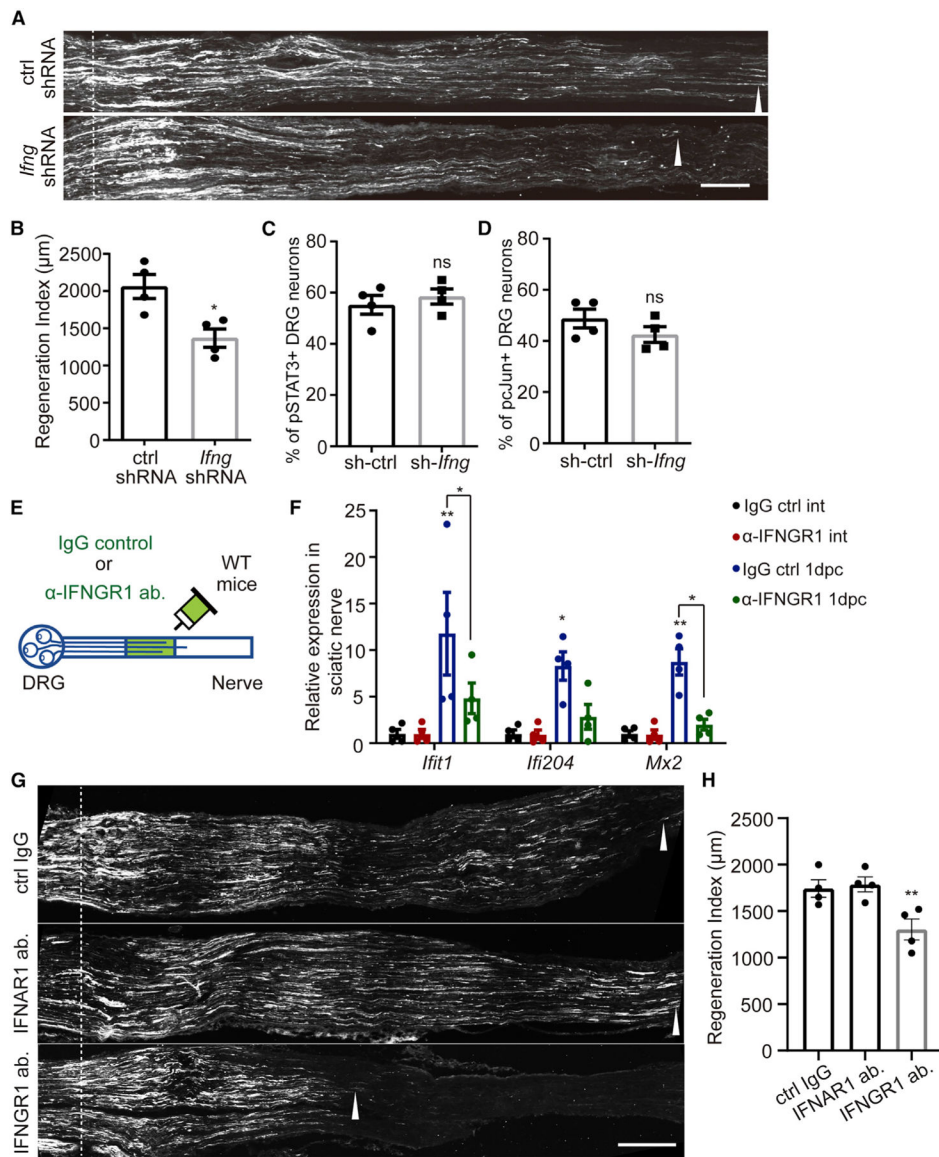Mean ± SEM; *p < 0.05, **p < 0.01. See also Figure S5.

Figure 6. Axonal IFNγ and its subsequent activation within the nerve are required for the peripheral axon regeneration

(A) Representative sections from sciatic nerves of WT animals with respective virus injection at 3 dpc. Regenerating axons were visualized by SCG10 staining. Dotted lines indicate the proximal side of the lesion site and arrowheads indicate the terminals of longest regenerating axons. Scale bar, 200 μm.

(B) Quantification of sensory axon regeneration in (A). Student's t test, n = 4 mice.

(C) Quantification of percentages of pSTAT3 positive DRG neurons at 3 dpc. Sciatic nerve crush was done 4 weeks after AAV-ctrl or Ifng-shRNA injection. ns, not significant, Student's t test, n = 4 mice.

(D) Quantification of percentages of pcJun positive DRG neurons at 3 dpc. Sciatic nerve crush was done 4 weeks after AAV-ctrl or Ifng-shRNA injection. ns, not significant, Student's t test, n = 4 mice.

(E) A diagram shows the method of sciatic nerve injection of antibody.

(F) qPCR analysis of ISG expression in at 1 dpc. Ctrl or IFNGR1 antibody was injected into the sciatic nerve after injury. ANOVA followed by Tukey's test, n=4 mice.

(G) Representative sections from sciatic nerves of WT animals with respective antibody injection at 3 dpc. Scale bar, 200 μm.

(H) Quantification of sensory axon regeneration of respective groups in (G). ANOVA followed by Dunnett's test, n = 4 mice. Mean ± SEM; *p < 0.05, **p < 0.01. See also Figure S6.
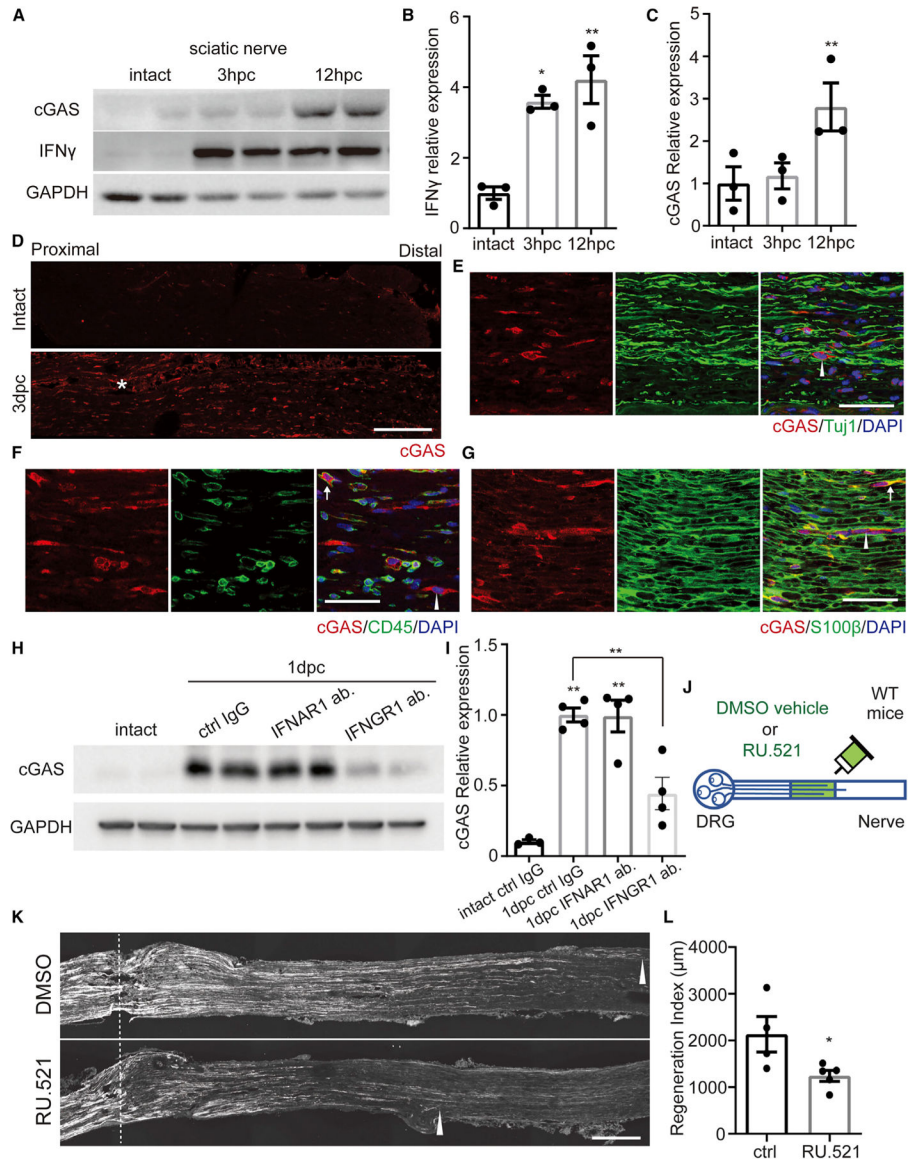
Figure 7. Axonal IFNγ upregulates cGAS in the non-neuronal cells of the sciatic nerve to promote regeneration

(A) Western blots of IFNγ and cGAS in sciatic nerve lysate at different time points after injury.

(B) Quantification of IFNγ expression level in (A). ANOVA followed by Dunnett's test, n = 3 mice.

(C) Quantification of cGAS expression level in (A). n = 3 nerves. ANOVA followed by Dunnett's test, n = 3 mice.

(D) Sections of intact or 3 dpc sciatic nerves from WT animal, stained with cGAS (red) antibody. Asterisk labels the lesion site. Scale bars, 200 μm.

(E) Section of a sciatic nerve from WT animal at 3 dpc was stained with Tuj1 (green) and cGAS (red). Arrowhead labels cGAS+/Tuj1— cells. Scale bars, 50 μm.

(F) Section of a sciatic nerve from WT animal at 3 dpc was stained with CD45 (green) and cGAS (red). Arrow labels double-positive cells and arrowhead labels cGAS+/CD45— cells. Scale bars, 50 μm.

(G) Section of a sciatic nerve from WT animal at 3 dpc was stained with S100b (green) and cGAS (red). Arrow labels double-positive cells and arrowhead labels cGAS+/ S100b— cells. Scale bars, 50 μm.

(H) Western blots of cGAS in sciatic nerve lysate at 1 dpc. Ctrl, IFNAR1 or IFNGR1 neutralizing antibodies were injected into the sciatic nerve after injury.

(I) Quantification of cGAS expression in (H). n = 3–4 nerves. ANOVA followed by Dunnett's test.

(J) A diagram shows the method of sciatic nerve injection of DMSO vehicle or RU.521.

(K) Representative sections from sciatic nerves of WT animals with DMSO vehicle or RU.521 injection. Scale bars, 200 μm.

(L) Quantification of sensory axon regeneration in (K). Student's t test, n = 4–5 mice. Mean ± SEM; *p < 0.05, **p < 0.01. See also Figure S7.

Figure 8. cGAMP promotes peripheral axon regeneration through axonal STING

(A) Representative images of DRG neurons in primary cultures treated with DMSO vehicle, cGAMP (10 μM), DMXAA (10 μM), C-176 (1 μM), or H-151 (1 μM). Scale bar, 400 μm.

(B) Quantification of lengths of the longest axon for each DRG neuron in (A). n = 3 mice. ANOVA followed by Dunnett's test.

(C) Representative images of DRG neurons from WT, *Sting* KO, or *Mavs* KO mice in primary cultures treated with DMSO vehicle or cGAMP (10 μM). Scale bar, 400 μm.

(D) Quantification of lengths of the longest axon for each DRG neuron in (C). n = 3 mice. ANOVA followed by Tukey's test.

(E) Representative sections from sciatic nerves of WT animals with DMSO or H151 (1 μM) injection at 3 dpc. Scale bar, 200 μm.

(F) Quantification of sensory axon regeneration in (E). Student's t test, n = 4 mice.

(G) Representative images of embryonic DRG culture in the compartmented chamber treated with PBS or ADU-S100 (10 μM). Scale bar, 400 μm.

(H) Quantification of neurite lengths in (E). ANOVA followed by Dunnett's test, n = 6 batches of primary culture.

(I) Representative images of growth cones of EB1-GFP transfected DRG neurons treated with PBS or ADU-S100 (10 μM). Scale bar, 5 μm.

(J) Quantification of growth cone area in (I). Each dot represents a DRG neuron. Student's t test, n = 20 cells.

(K) Quantification of EB1-GFP intensity in (I). Each dot represents a DRG neuron. Student's t test, n = 20 cells.

(L) Kymograph showing EB1-GFP comet tracking in live cell imaging in (I).

(M) Quantification of highest EB1-GFP comet velocity during 2 min live imaging. Each dot represents a single EB1-GFP comet. Student's t test, n = 65 for control group and 144 for ADU-S100 group.

Mean ± SEM; *p < 0.05, **p < 0.01. See also Figure S8.